Materials Science and Engineering R 70 (2010) 275–302

Contents lists available at ScienceDirect

Materials Science and Engineering R

journal homepage: www.elsevier.com/locate/mser

Surface nano-functionalization of biomaterials

Xuanyong Liu [a,b,**], Paul K. Chu [b,*], Chuanxian Ding [a,*]

[a] Key Laboratory of Inorganic Coating Materials, Shanghai Institute of Ceramics, Chinese Academy of Sciences, Shanghai 200050, China
[b] Department of Physics & Materials Science, City University of Hong Kong, Tat Chee Avenue, Kowloon, Hong Kong, China

ARTICLE INFO

Keywords:
Biomaterials
Surface
Nano-functionalization
Review

ABSTRACT

After biomaterials are implanted into the human body, there are inevitable interactions between the biological environment and implant surfaces. Therefore, the surface of biomaterials has become one of the hottest research topics. Nanotechnology is a powerful tool in modern materials science and able to incorporate biomimicry on the nanoscale into materials engineering. Therefore, research on nanotechnology/nanostructured biomaterials has attracted much attention. A nano-functionalized surface has promising biological properties and clinical applications of biomaterials can be improved by producing a nanostructured surface. Many surface modification techniques have been adopted to produce nano-functionalized biomaterials surface, and in this paper, the fabrication, characterization, and properties of biomaterials such as ceramics, metals, and polymers with nanostructured surfaces are reviewed.

Contents

1. Introduction

It is well known that a series of interactions occur between the surface of biomaterials and the biological environment after they have been implanted into the human body. Therefore, the biomaterials surface plays an extremely important role in the

* Corresponding authors. Tel.: +86 21 52412409; fax: +86 21 52412409.
** Corresponding author at: Key Laboratory of Inorganic Coating Materials, Shanghai Institute of Ceramics, Chinese Academy of Sciences, Shanghai 200050, China. Tel.: +86 21 52412409; fax: +86 21 52412409.
E-mail addresses: xyliu@mail.sic.ac.cn (X. Liu), paul.chu@cityu.edu.hk (P.K. Chu), cxding@sunm.shcnc.ac.cn (C. Ding).

0927-796X/$ – see front matter © 2010 Elsevier B.V. All rights reserved.
doi:10.1016/j.mser.2010.06.013

response of artificial medical devices to the biological environment. The efficacy of artificial implants is determined mainly by their surface characteristics such as surface morphology, microstructure, composition, and properties. These properties alter adsorption of proteins which mediate the adhesion of desirable and undesirable cells [1]. Research on biomaterials surface has become one of the hottest topics in biomaterials and biomedical engineering. The highest score for a keyword in the World Biomaterial Congress in 2008 (WBC 2008) is *Biomaterials Surface*, indicating that the current research focus of the biomaterials community is aimed at understanding the fundamental processes at the interface between implant surfaces and surrounding living tissues. It is also generally agreed that human biology and nature should be considered in the design of functionalized biomaterials [2].

Nanotechnology has become a powerful tool in modern materials science. It is able to incorporate biomimicry on the nanoscale into materials engineering. Research on nanotechnology/nanostructured biomaterials is also one of the hottest topics in the biomaterials field and in fact, "nanotechnology/nanostructured biomaterials" are also very important keywords in WBC 2008. Nanoscale materials are thought to interact with some proteins more effectively than conventional materials. For instance, osteoblast functions are mediated due to their similar size and altered energetics. Balasundaram and Webster [1] suggest that nanophase materials may be alternative orthopedic implant materials because of their ability to mimic the dimensions of the constituents and components in natural bone-like proteins and hydroxyapatite. Nanofibers with shape resembling hydroxyapatite crystals in bones can influence the conformation of typical adhesive proteins such as fibronectin and vitronectin as well as osteoblast behavior [3,4]. Some other nanostructures that spur enhanced response from osteoblasts and subsequently more efficient deposition of calcium-containing minerals include nanometals, carbon nanofibers and nanotubes, nanopolymers, and nanocomposites of ceramics and polymers. A number of studies have been conducted to evaluate the nanomaterials chemistry and preliminary results suggest that increased bone cell functions may be independent of the bulk materials chemistry but rather rely on the degree of the nanostructured surface roughness [5–8].

A nano-functionalized surface has promising biological properties. Hence, clinical applications of biomaterials can be improved by producing a nanostructured surface. Surfaces that contain microscale and nanoscale features in a well-controlled manner have been shown to significantly affect cellular and subcellular functions [9]. In this paper, recent work on the fabrication, characterization, and properties of biomaterials including ceramics, metals, and polymers with nanostructured surfaces is reviewed.

2. Nanostructures in nature

Many nanostructures can be found in nature [10]. For example, the surface of lotus leaves is composed of micro- and nano-scale hierarchical structures composed of fine-branched nanostructures (ca. 120 nm) on top of micropapillae (5–9 μm) as shown in Fig. 1 [11,12]. Scanning electron microscopy (SEM) reveals that on the lotus leave surface, every epidermal cell forms a micrometer-scale papilla and has a dense layer of epicuticular waxes superimposed on it. Each of the papillae consists of branchlike nanostructures. The synergistic effects between these special double-scale surface structures and hydrophobic cuticular waxes are thought to be the reason for the super-hydrophobicity as indicated by a high water contact angle and low sliding angle. As another example, butterflies [13] and cicadae [14] can keep themselves uncontaminated by removing dust particles, dew, or water droplets easily from their wings spontaneously. Such properties also originate from the special structures on their wings. The cicada wing is composed of aligned nanocolumns with diameters of about 70 nm and a column-to-column distance of about 90 nm, as shown in Fig. 2. These surface microstructures bestow the wing with its self-cleaning property.

Nanostructures also exist in the human body. For example, the size of ions, DNA, proteins, and virus in the human body ranges from several nanometers to sub-micrometers. Human bones are composed of nanosized organic and mineral phases agglomerating to form a large macrostructure. Proteins present in the extracellular matrix of bones are nanostructured comparable to collagen fibrils. Furthermore, tiny mineral particles composed of calcium phosphate, an important constituent of the bone matrix, is compositionally and structurally nanostructured. A sketch of the most probable arrangement of the mineral particles with respect to the collagen molecules is shown in Fig. 3 [15].

3. Surface nano-functionalization technologies of biomaterials

Nanostructured surfaces can be produced on conventional biomaterials by surface modification. Depending on the ways surfaces are modified, nano-functionalization techniques can be categorized into two groups, namely nano coating and film deposition as well as *in situ* surface nano-functionalization, as illustrated in Fig. 4a and b. These two types of techniques are often combined to produce surfaces with hybrid nanostructures such as a coating/film and a nanostructured zone (Fig. 4c). Typical coating and film deposition techniques are plasma spraying, plasma immersion ion implantation & deposition (PIII&D), sol–gel, chemical vapor deposition (CVD), physical vapor deposition (PVD), cold spraying, self-assembly, and so on, whereas *in situ* surface modification techniques include laser etching, shot

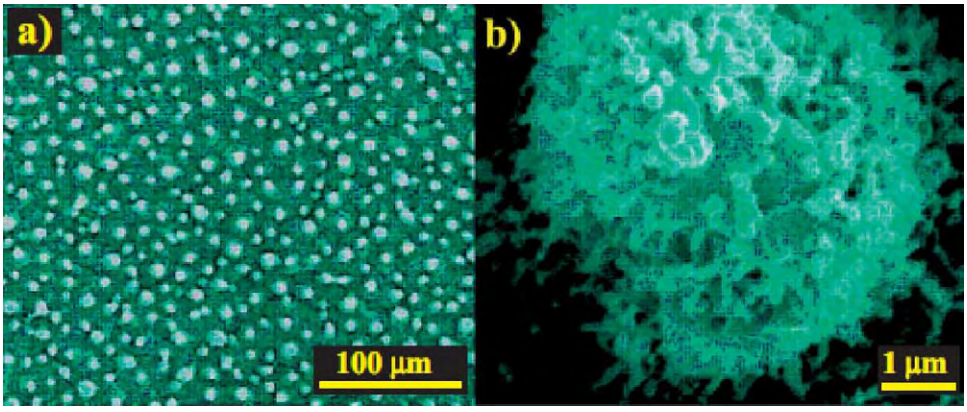

Fig. 1. Superhydrophobic lotus leaf: (a) low- and (b) high-magnification SEM images of the surface structures on the lotus leaf [11].

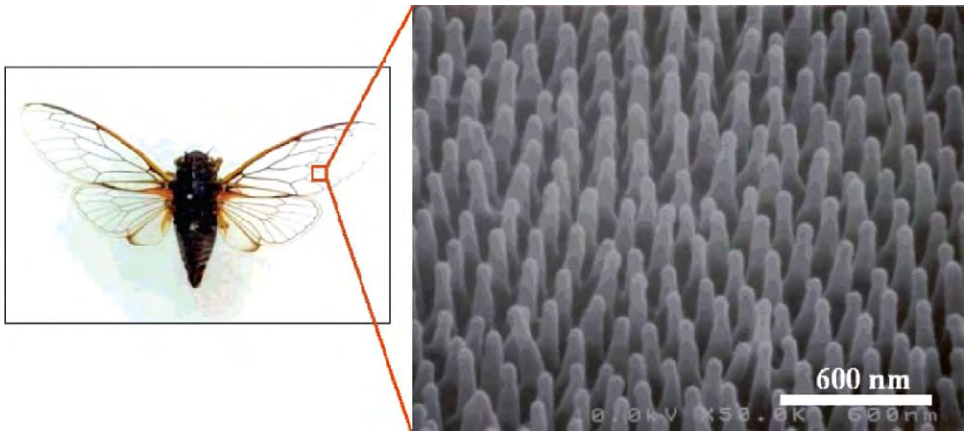

Fig. 2. Cicada orni (a) and field-emission SEM micrograph of the surface nanostructure on its wing surface [14].

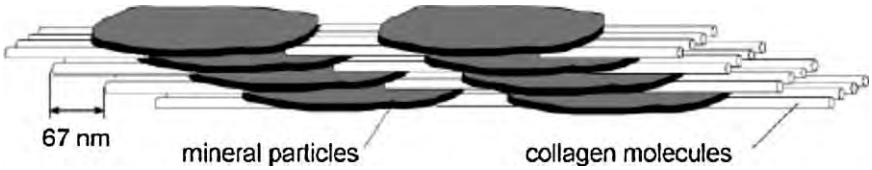

Fig. 3. Schematic of the arrangement of mineral particles in collagen fibrils—Mineral particles are typically very thin objects (2–4 nm) and aligned with the collagen matrix. Particles are believed to be nucleated at sites which are in register with the 67 nm period of the axial stagger of collagen molecules [15].

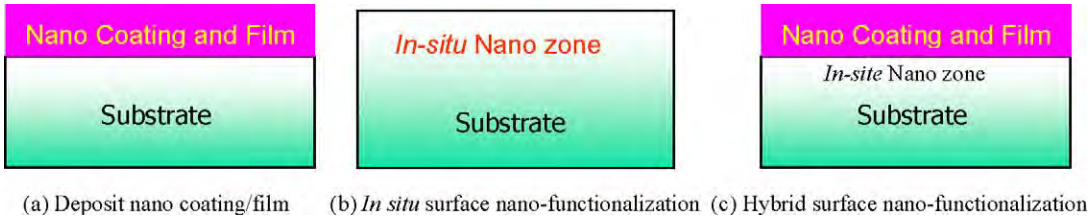

Fig. 4. Schematic diagram of surface nano-functionalization techniques.

blasting, acid and alkali treatments, anodic oxidation, micro-arc oxidation, ion implantation, etc. They will be reviewed here and more detailed descriptions of some of these techniques can be found in our previous review on surface modification of titanium [16].

4. Surface nano-functionalization of bioceramics

Conventional ceramic materials such as alumina, zirconia, titania, hydroxyapatite (HA), and calcium silicate with grain sizes larger than 100 nm possess good biocompatibility. However, clinical applications of these ceramics still encounter many difficulties because of insufficient bonding to the juxtaposed bone during prolonged use in the human body. In addition, applications to mend large bone defects are not yet feasible because of the intrinsic brittleness of ceramics. Therefore, development of novel and suitable ceramic materials that can promote and sustain osseo-integration with surrounding bones is crucial to wider orthopedic implant applications.

The influence of nanometer scale grain size of ceramics on bone cell adhesion has been investigated by Webster et al. [17]. The results indicate that osteoblast adhesion on nanophase alumina (23 nm grain size) and titania (32 nm grain size) is significantly greater than that on conventional alumina (177 nm grain size) and titania (2.12 μm grain size), respectively. Their work, which suggests a critical grain size for osteoblast adhesion between 49 and 67 nm for alumina and 32 and 56 nm for titania, provides evidence about the ability of nanophase alumina and titania to simulate the desirable materials characteristics of bones in a physiological environment, particularly those associated with the enhancement of protein interactions such as adsorption, configuration, and bioactivity as well as subsequent osteoblast adhesion. Webster et al. [18] have also investigated selected functions of osteoblasts on nanophase alumina, titania, and hydroxyapatite using *in vitro* cellular models. Compared to conventional ceramics, surface occupancy of osteoblast colonies is observed to be significantly less on the nanophase ceramics after 4 and 6 days of culturing. Osteoblast proliferation is also significantly greater on nanophase alumina, titania, and HA than on conventional ceramics after culturing for 3 and 5 days. Moreover, synthesis of alkaline phosphatase and deposition of calcium-containing minerals by osteoblasts cultured on the nanophase materials are significantly enhanced compared to conventional ceramics after 21 and 28 days. These results provide the first evidence of enhanced long-term (on the order of days to weeks) functions of osteoblasts cultured on nanophase ceramics. Consequently, it is generally accepted that nanophase ceramic materials present a unique and promising class of orthopedic/dental implants with improved osseo-integrative properties.

Events at the tissue-implant interface that mediate osteoclast functions and consequently the degree of resorption and formation of new bones around prostheses determine the efficacy of orthopedic/dental implants. Therefore, it is very important to

investigate the functions of osteoclast-like cells on implant materials. Webster et al. [19] have investigated the synthesis of tartrate-resistant acid phosphatase (TRAP) and formation of resorption pits by osteoclast-like cells and bone-resorbing cells on nanophase alumina and HA *in vitro*. Compared to conventional ceramics, synthesis of TRAP by osteoclast-like cells cultured on nanophase alumina and nanophase HA is enhanced significantly after 10 and 13 days. Formation of resorption pits by osteoclast-like cells cultured on nanophase alumina and nanophase HA is also much higher after 7, 10, and 13 days. In addition, Webster's group has conducted a series of experiments studying the effects of nanophase ceramics and fibers on the functions of osteoblast-like cells. The results provide more evidence on enhanced osteoblast-like cell functions on nanophase ceramics [6,20–24].

On account of their impressive structural, electrical, and mechanical properties as well as small size and mass, carbon nanotubes (CNTs) have become one of the most promising materials and opened a new era in materials science and nanotechnology. In recent years, considerable efforts have been devoted to applying CNTs to the biological and medical fields due to not only their ability to simulate dimensions of proteins that comprise native tissues but also their higher reactivity in interactions involving cell attachment [25,26]. Boccaccini et al. [27] have deposited uniform CNTs on highly porous bioactive and biodegradable 45S5 Bioglass®-derived glass-ceramic scaffolds intended for bone tissue engineering by electrophoretic deposition. The aims of their work are to stimulate osteoblast cell attachment and proliferation by providing a nanostructured surface consisting of pore walls and to confer biosensing properties to scaffolds by adding electrical conduction functions. By studying the formation of hydroxyapatite crystals on the surface of the CNT coated Bioglass® scaffolds during immersion in SBF, it has been confirmed that the bioactivity of the scaffolds is not impaired by the presence of CNTs. The results suggest that CNTs can induce orderly formation of a nanostructured CNT/HA composite layer when scaffolds are in contact with biologically relevant media.

5. Surface nano-functionalization of biomedical metals

It has been demonstrated that metal surfaces with low-micrometer to nanophase topography enhance adhesion of osteoblasts. Ward et al. [28] have investigated the enhanced functions of osteoblasts on nanophase metals and indicated that both calcium and phosphorous are deposited on the Ti, Ti6Al4V, and CoCrMo substrates. Compared to conventional metals, more calcium and phosphorus deposition are observed on the surface of nanophase metals. Nanophase CoCrMo shows the largest amounts of deposited calcium and phosphorus compared to other metal substrates, which gives evidence that nanophase metals are desirable in orthopedic implants. The nano-functionalized surfaces also possess promising biological properties and therefore, the biological properties and clinical applications of titanium, titanium alloys, and related materials can be improved and widened by producing a nanostructured surface. In the past ten years, much work was performed on surface nanofunctionalization of titanium. Coatings and films with nanostructures such as nanograins, nanopores, nanotubes, nanopartices, nanowires, and nanorods have been synthesized on titanium and its alloys using various surface modification techniques such as chemical treatment, anodic oxidation, micro-arc oxidation, sol–gel, plasma spraying, surface mechanical attrition treatment (SMAT), physical vapor deposition, and chemical vapor deposition.

5.1. Chemical treatment

Chemical treatments using acids, alkalis, and hydrogen peroxide involve chemical reactions at the interface between the materials and solution. They are considered enabling techniques from the viewpoint of surface modification of biomaterials, especially metals, due to the simplicity and flexibility. Titanium and Ti alloys are generally encapsulated by a native protective oxide film typically composed of three different layers, TiO (inner layer in contact with the metal), Ti_2O_3 (intermediate layer), and TiO_2 (outer layer) as shown in Fig. 5a. [29]. When titanium is immersed in an oxidizing solution, a chain of reactions occurs to form nanostructures on the surface (Fig. 5b) [30]. The suboxides, TiO, and Ti_2O_3 are transformed into TiO_2 in the oxidizing medium while the etching solution penetrates the nanopits and reaches the underlying metal. Hence, passivation layers are naturally created. The native layered structure composed of TiO (in contact with the metal), Ti_2O_3 (intermediate), and TiO_2 (outer layer) is reestablished. The oxidation process increases the amount of TiO_2 to the extent that the underlying suboxides can no longer be detected but the layer organization is not altered.

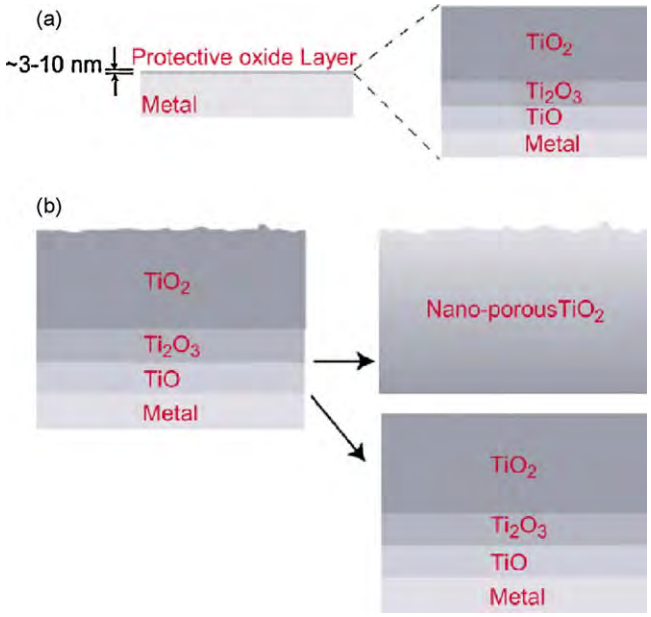

Fig. 5. Schematic representation of the layered structure (a) before (native oxide) and (b) after chemical oxidation [30].

When Ti and Ti alloys undergo alkali and heat treatments, the surfaces are modified in several stages as shown in Fig. 6 [31]. During the alkali treatment, the native protective oxide film on the surface partially dissolves into the alkaline solution because of corrosive attack by hydroxyl groups while hydration of Ti metal proceeds simultaneously. Negatively charged hydrates such as $HTiO_3^- \cdot nH_2O$ produced on the substrate surface combine with alkali ions from the aqueous solution to form an alkali titanate hydrogel layer. During the heat treatment, the hydrogel layer is dehydrated and densified to form a stable amorphous or crystalline alkali titanate layer.

A surface with various nanostructures can be obtained by chemically treating titanium and its alloys. Chemical treatments are suitable for the creation of micrometer-scale and nanometer-scale textures on large-area surfaces and multifaceted devices with complex 3D shape due to the non-line-of-sight nature. Wu et al. [32,33] have produced titania nanorods at low temperature on a large scale via direct oxidation of titanium with hydrogen peroxide. The ordered nanorod layer with a thickness of approximately 1 μm is deposited on a 2 μm thick condensed anatase layer as illustrated by Fig. 7. Most of the as-deposited nanorods have mixed anatase and rutile phases and the nanorods grow along the rutile [0 0 1]-axis direction. Wu et al. [34] have also

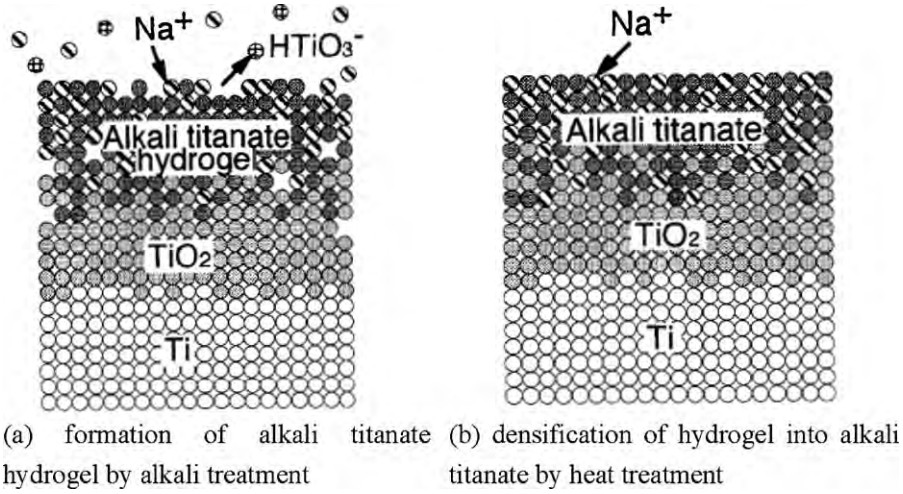

Fig. 6. Schematic representation of surface structural change on Ti metal: (a) in the presence of alkali and (b) heat treatment [31].

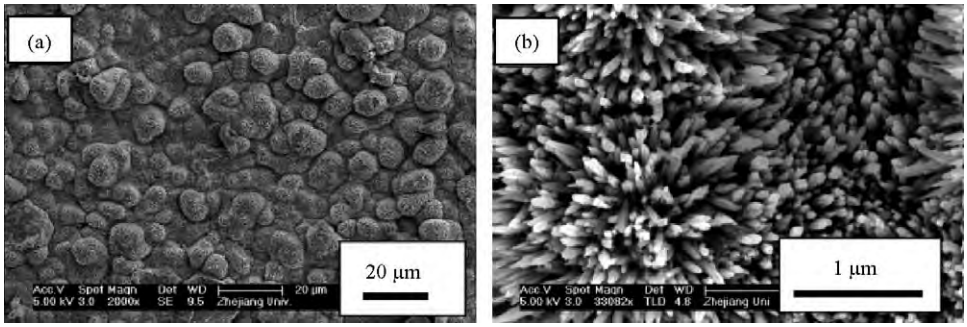

Fig. 7. SEM images of a titania nanorod formed on titanium substrate: (a) low magnification, (b) high magnification [33].

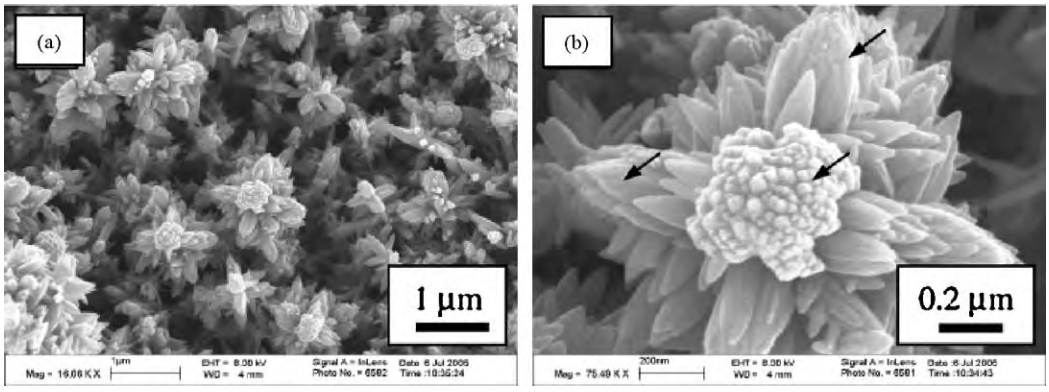

Fig. 8. SEM views of a titania nanoflower obtained by oxidation of Ti in 30 wt% H_2O_2 solutions containing 0.014 M hexamethylenetetramine and 0.4 M, followed by heating at 400 °C for 1 h: (a) low magnification, (b) high magnification [34].

reported the synthesis of titania nanoflowers by oxidizing pure titanium in hydrogen peroxide solutions containing hexamethylenetetramine and nitric acid at a low temperature of 353 K (Fig. 8). Titania nanoflowers possessing mainly the anatase structure together with a mixture of anatase and rutile phases are obtained after subsequent thermal treatment to crystallize the as-precipitated amorphous structure.

Titania nanowire arrays have been fabricated by Wu et al. [35]. Here, hydrogen peroxide solutions containing melamine and nitric acid are used to react with Ti at a low temperature of 353 K for 72 h, followed by thermal treatment at 723 K for 1 h. The titania nanowires are anatase with a mean diameter of 25 nm and an aspect ratio of about 40, as shown in Fig. 9. Other researchers have also synthesized anatase TiO_2 nanowire films by *in situ* oxidization of a Ti plate in a solution containing concentrated H_2O_2 and NaOH followed by proton exchange and calcination [36]. Hosono et al. [37] have developed a method to prepare perpendicular TiO_2 nanosheet films from titanate nanosheet films produced on a titanium metal sheet by a hydrothermal treatment in aqueous urea as illustrated in Fig. 10. The resulting anatase TiO_2 nanosheet films exhibit specific superhydrophilicity without the need of additional UV irradiation.

Chemical treatments are generally simple and effective and nanostructured Ti can be obtained without compromising its

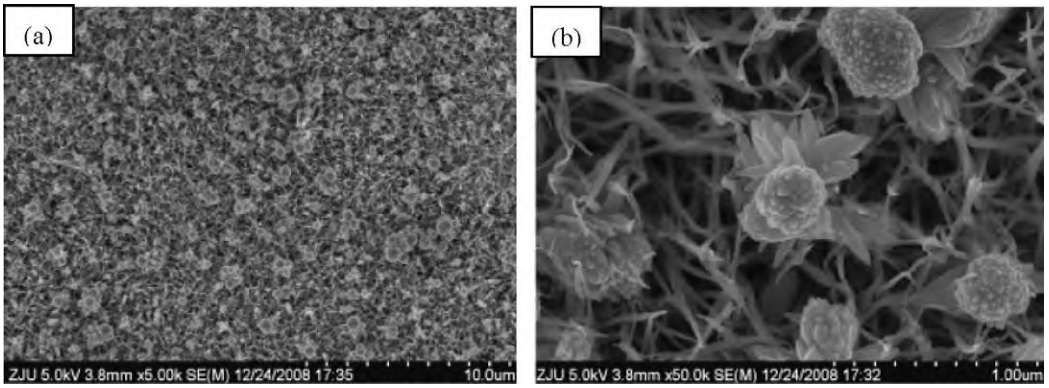

Fig. 9. SEM morphologies of titania thin film obtained by the oxidation of Ti in 30 wt% H_2O_2 solutions containing 2.4 mM melamine and 0.725 M HNO_3, followed by heating at 723 K for 1 h: (a) low magnification, (b) high magnification [35].

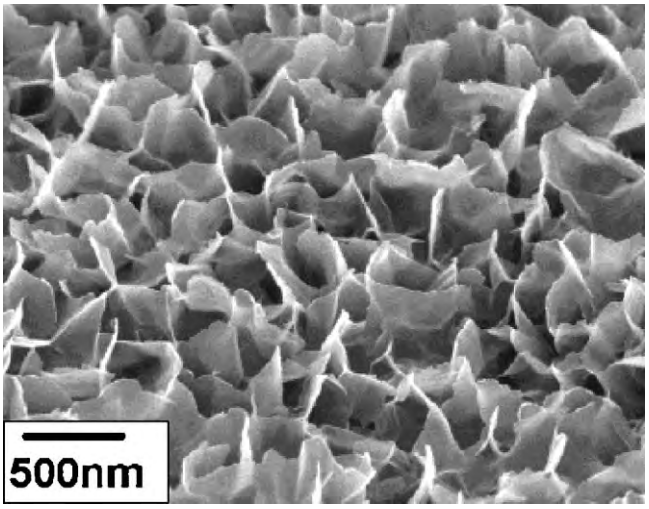

Fig. 10. SEM image of the perpendicular TiO_2 nanosheet film fabricated by heating the ammonium titanate film using the hydrothermal method in an urea solution at 400 °C for 30 min. [37].

biocompatibility. Therefore, studies on direct chemical treatments with acids, alkalis, and hydrogen peroxide have been widely conducted recently. The surface physicochemical characteristics and topographies obtained by these treatments can be carefully controlled to favor adhesion and proliferation of osteogenic cells [30,38], precipitation of apatite [39–41], and expression of bone-related genes and proteins [42].

Guo et al. [42] have shown that HF treatment of the TiO_2 grit blasted titanium surface renders the treated surface with nanometer scale features which enhance the osteo-conductivity of the adherent cells as well as bone specific mRNA expression. In addition, Lamolle et al. [43] have reported that surfaces with higher roughness, lower cytotoxicity level, and better biocompatibility can be produced on polished Ti surfaces by submerging Ti implants in a 0.2% HF solution while controlling the exposure time and initial surface topography carefully. It is believed that the favorable conditions for cell growth with improved biocompatibility stem from the low hydrocarbon content, presence of fluoride, hydride and oxide, and the micro and nano-topography created by the HF treatment.

Surface modification of Ti and Ti alloys using a mixture of acid and H_2O_2 has also attracted a great deal of attention. Lee et al. [40] have investigated whether surface modification affects the precipitation of apatite on titanium. The *in vitro* experiments show that apatite with a round pattern can precipitate on the surface after chemical and heat treatment. Moreover, the *in vivo* experiments show excellent biocompatibility as indicated by the small inflammation reaction and decrease in the average thickness of the fibrous capsule surrounding the metal specimens implanted into the connective tissue compared to the untreated titanium, aluminum, and stainless steel. This work confirms that titanium with superior biocompatibility can be obtained by specific chemical treatment. In addition, Variola et al. [30] discuss the feasibility of creating bioactive nano- and micro-textured surfaces on polished Ti-6Al-4V alloy by a simple treatment 22 °C using a mixture containing pure H_2SO_4 and 30% H_2O_2 with a ratio of 1:1 (vol.%). The physicochemical characteristics of these surfaces can be tailored by controlling the etching time. Interestingly, these surfaces exert selective effects on cells, as revealed by facilitated growth of osteogenic cells and limited growth of fibroblastic cells. The proposed reason is that the nanoporous oxidized Ti-alloy surfaces can provide cues to cells that engender specific cellular responses. With this unique property, these surfaces can influence different types of cells in a diverse way while addressing distinct situations, so that integration of implants with the host can be enhanced. Shi et al. [38] have recently reported that the H_2O_2/HCl and heat treatment may facilitate better integration between Ti-6Al-4V implants and bones by providing the bioactive surface with moderate surface roughness and a porous titania gel layer, which is important to adsorption of proteins and mineral ions as well as cell growth. Here, Ti-6Al-4V disks are sandblasted, etched with HF and HNO_3, treated by the H_2O_2/HCl mixture, and heated. The samples consist of sandblasted, dual acid-etched disks as the control group as shown in Fig. 11. Proliferation and differentiation of preosteoblast cells on these two groups are investigated *in vitro*. Mouse preosteoblasts (MC3T3-E1 cells) are cultured and examined after 4 days, 7 days, and 14 days. The alkaline phosphatase (ALP) activity and osteocalcin (OC) production observed from the test group are much higher than those determined from the control group at every time point investigated. Furthermore, in the test group, the expressions of alkaline phosphatase-2, osteocalcin, and collagen type I alpha 1 mRNAs are significantly up-regulated.

Uchida et al. [44] have prepared a laminin-apatite composite layer on the surface of titanium without denaturation of the laminin using biomimetic processes and investigated its cell adhesive properties. Here, NaOH- and heat-treated titanium metal is used as the base materials and immersed the laminin-containing calcium phosphate solution to produce a laminin-apatite composite thin layer because this process can induce apatite nucleation and growth on the surface in the physiological environment. The results show that titanium coated with a laminin-apatite composite coating exhibits excellent adhesion to epithelial cells. Therefore, the authors expect that these materials can prevent

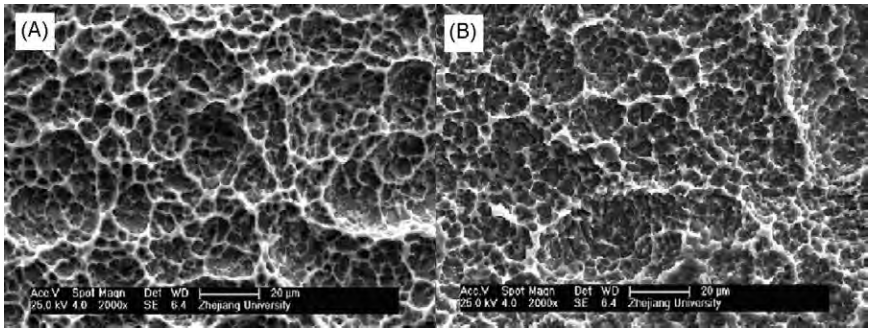

Fig. 11. SEM images of two different Ti alloy surfaces: (A) The sandblasted, dual acid-etched and H_2O_2/HCl heat-treated Ti-6Al-4V disc (test group) has an irregular surface with porous network structure. (B) The sandblasted, dual acid-etched treated Ti-6Al-4V disc (control group) has a similar surface. However, the micropits and indentations on this surface seem a little smaller compared to those on the test surface [38].

bacterial infection and be useful in percutaneous implants such as artificial tooth roots or skin terminals. In addition, it is believed that the biomimetic-coating process can incorporate other functional proteins on the surface of materials that have apatite-forming ability in the body environment.

Wu, Chu et al. [45] have reported large-scale direct growth of nanostructured bioactive titanates on three-dimensional (3D) microporous Ti-based metal (NiTi and Ti) scaffolds by immersing the scaffold in a 10 M NaOH aqueous solution at 60 °C inside a Teflon-lined autoclave (Fig. 12). The nanostructured titanates show characteristics of one-dimensional (1D) nanobelts/nanowires on a nanoskeleton layer. Besides resembling cancellous bone structure on the micro/macroscale, the 1D nanostructured titanate on the exposed surface is similar to the lowest level of hierarchical organization of collagen and hydroxyapatite. The resulting surface displays superhydrophilicity, favors deposition of hydroxyapatite, and accelerates cell attachment and proliferation.

Direct chemical treatments have also been utilized to modify biomedical materials other than Ti and its alloys. Miyazaki et al. [46] have reported that tantalum can form apatite on the surface in simulated body fluids in a short period after it has been previously treated in a diluted NaOH solution to form an amorphous sodium tantalate hydrogel layer on the tantalum surface. This indicates the possibility of obtaining bioactive tantalum metal by simple chemical treatments. Uchida et al. [47] in the same group also confirm the possibility of obtaining bioactive zirconium after treatment with NaOH. Zirconium metals processed in NaOH aqueous solutions with concentrations above 5 M can form an apatite layer on the surface in simulated body fluids. Apatite nucleation is induced by the Zr–OH groups in the zirconia hydrogel layer which forms on the metal surface upon exposure to the NaOH solution.

5.2. Anodic oxidation

Anodic oxidation encompasses electrode reactions in combination with electric field driven metal and oxygen ion diffusion leading to the formation of an oxide film on the anode surface.

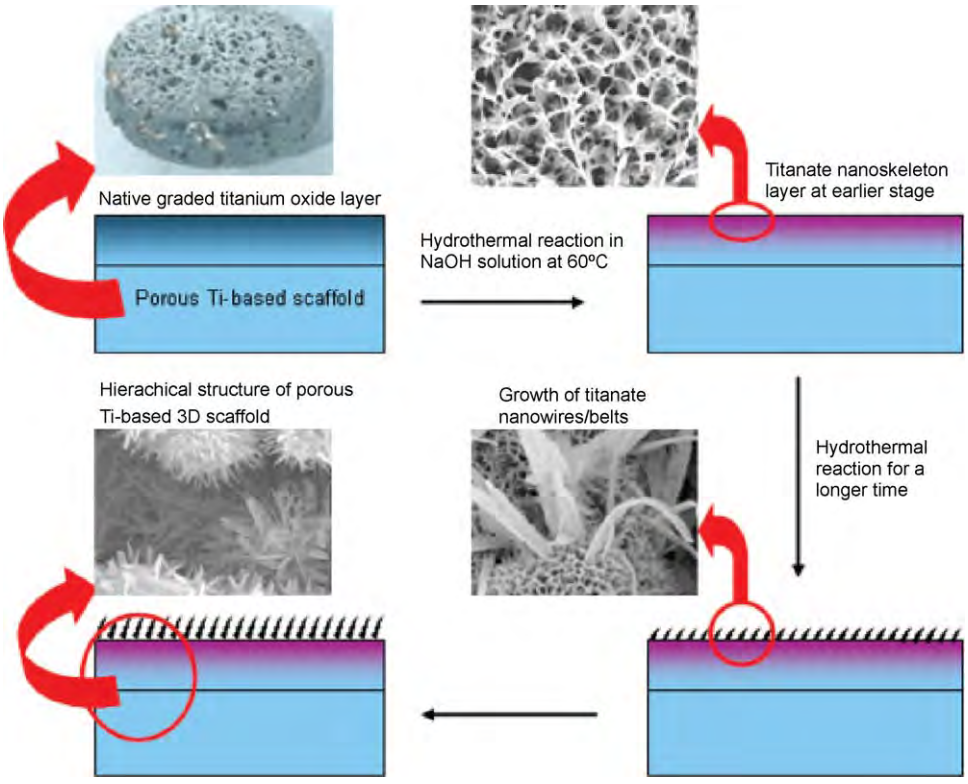

Fig. 12. Schematic diagram of the fabrication process of a hierarchical 3D porous Ti-based metal scaffold in a 10 M NaOH aqueous solution at a low temperature [45].

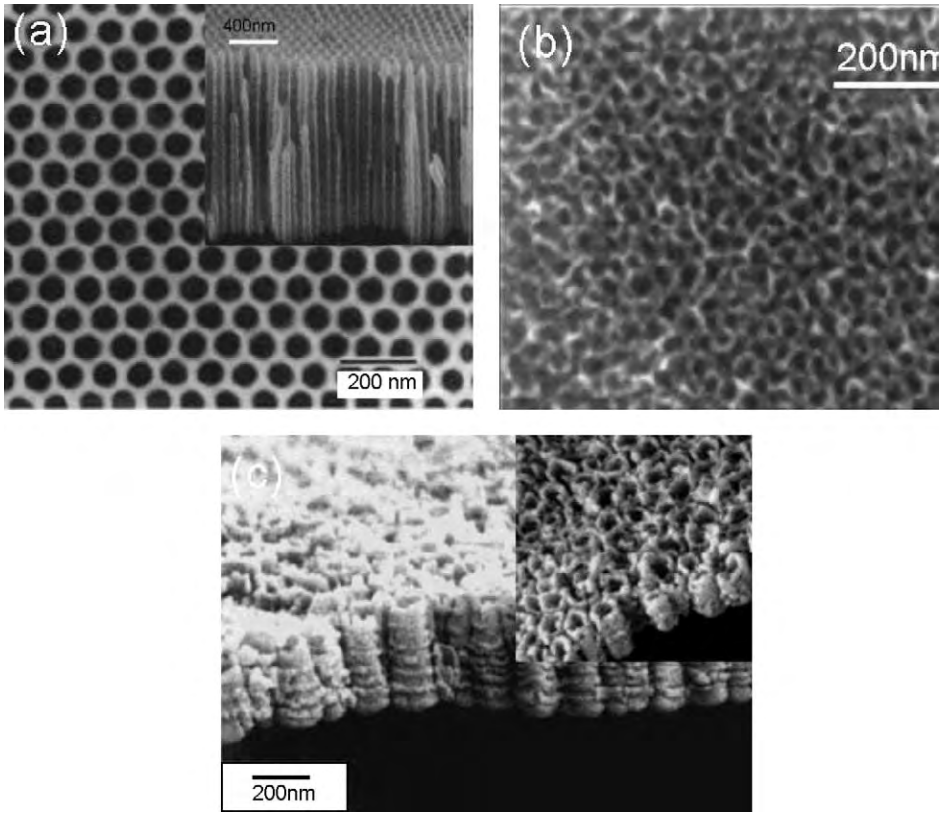

Fig. 13. (a) SEM photographs of the anodic alumina. View of the surface and inset is the cross-sectional view [48]; (b) High-resolution scanning electron micrographs of anodic oxide films grown on titanium at 5 V for 20 min [49]; (c) FE-SEM cross-sectional images of titanium oxide nanotubes. The sample is anodized in a 0.5 wt% HF solution at 20 V for 20 min [50].

Anodic oxidation is a well established method to produce different types of protective oxide films on metals and different diluted acids (H_2SO_4, H_3PO_4, acetic acid and others) can be used as electrolytes in the process. Although anodic oxidation has been known for more than 50 years, it was until 1995 when Masuda and Fukuda [48] demonstrated that an oxide formed by highly ordered pore arrays could be produced by optimizing the anodization conditions (Fig. 13a). Anodization is recognized as a self-ordering electrochemistry approach to form some nanoscale structures. In 1999, Zwilling et al. [49] were the first to obtain self-ordered TiO_2 nanostructures by anodizing Ti in a fluoride containing electrolyte (Fig. 13b). In 2001, Gong et al. [50] fabricated well aligned and organized TiO_2 nanotubes by anodization of a pure titanium sheet in an aqueous HF electrolyte (Fig. 13c).

It is generally agreed that the formation of TiO_2 nanotube arrays in a fluoride containing electrolyte is the result of two competing electric field-assisted processes [51,52]. The first process is the oxidation of the Ti metal to form a passive TiO_2 layer:

$$Ti + 2H_2O \rightarrow TiO_2 + 4H^+ + 4e^-,$$

and the second process is the chemical dissolution of the formed TiO_2 oxide by the following reaction:

$$TiO_2 + 4H^+6F^- \rightarrow [TiF_6]^{2-} + 2H_2O.$$

These nanotube structures are produced in a controlled manner by optimizing parameters including anodization potential, electrolyte composition and properties such as pH, conductivity, viscosity, as well as anodization time and temperature [53–58]. Some high aspect ratio [53], smooth [54], ultra-long [55], and special nanostructures like double-walled [56] and bamboo-type nanotubes [57] have been synthesized as shown in Fig. 14a–e. The methodology has been applied to other valve metals [59] such as Hf, Ta, W, Nb, Zr and their alloys like TiNb, TiZr, TiAl, Ti6Al7Nb, Ti6Al4V and Ti29Nb13Ta4.6Zr, as shown in Fig. 14f.

Anodic oxidation is generally a simple, versatile, and low-cost technique to produce nanostructures (nanoporous and nanotubes) on the surface of titanium. It has also been applied to form biomedical implants with highly ordered TiO_2 nanotube arrays that offer both biocompatibility as well as a unique surface nanostructure. It is necessary to review the use of TiO_2 nanotube arrays to enhance apatite formation and applications of TiO_2 nanotubular membranes for cell adhesion and growth. Tsuchiya et al. [60] have investigated the growth of hydroxyapatite formed on different TiO_2 nanotube layers. The results disclose that the presence of the nanotubes on a titanium surface enhances apatite formation and a 2 μm thick nanotube layer triggers deposition faster than the thinner layers. Tubes annealed to become anatase or a mixture of anatase and rutile are more efficient in promoting apatite formation than the tubes in their "as-formed" amorphous state. Kunze et al. [61] further confirm enhanced apatite deposition on titania nanotubes. Their results suggest that more nuclei form on the nanotubular surface than on flat compact TiO_2 in the initial stage of apatite growth. The nanotubular morphology combined with an anatase structure leads to the formation of apatite layers with a thickness of more than 6 nm in less than 2 days (Fig. 15).

There has been more speculation recently on the interactions between living cells and nanotubular layers of TiO_2. Park et al. [62] have studied the effects of the tube diameter on adhesion, spreading, growth, and differentiation of mesenchymal stem cells (MSCs). A spacing less than 30 nm with a maximum at 15 nm provides an effective length scale for accelerated integrin clustering/focal contact formation and strongly enhances cellular activities compared to smooth TiO_2 surfaces. Cell adhesion and spreading are severely impaired on nanotube layers with a tube

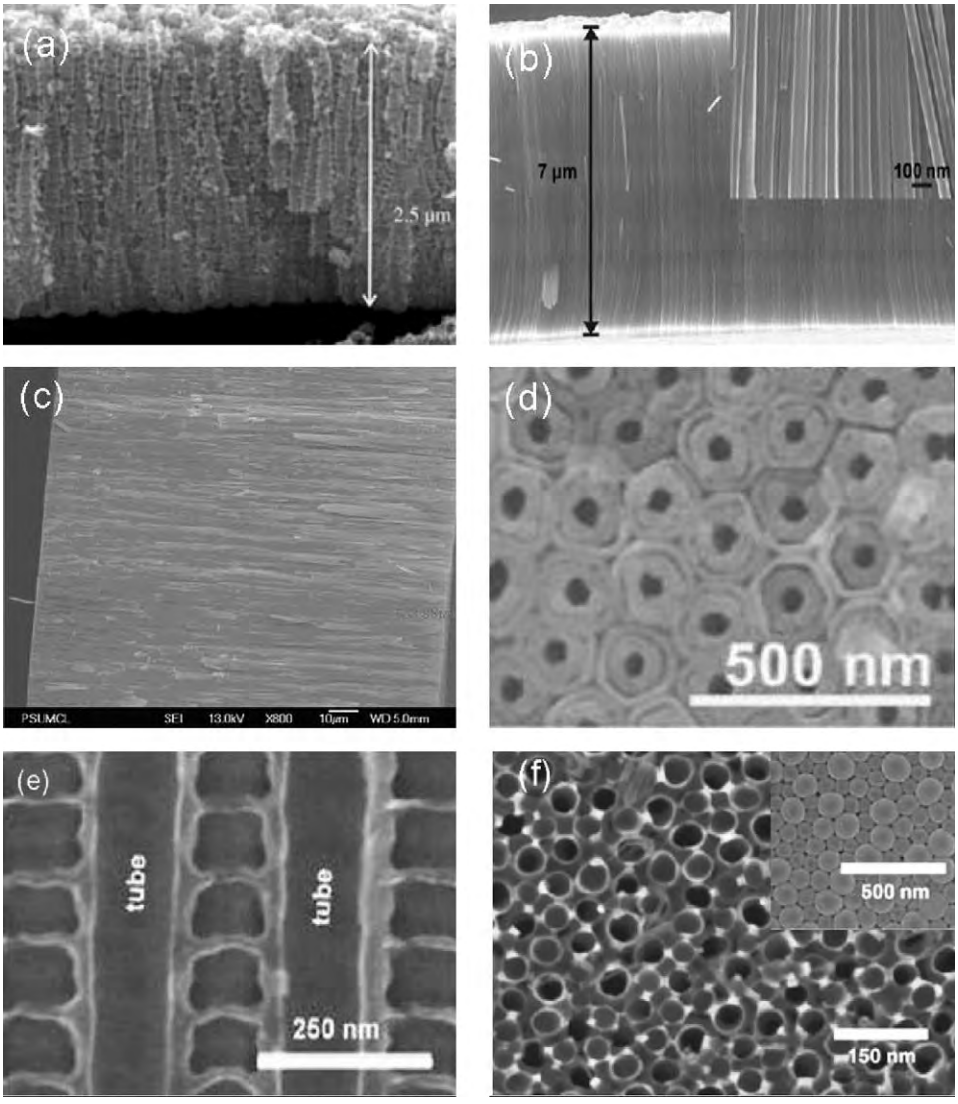

Fig. 14. (a) Cross-sectional views of a 2.5 μm thick self-organized porous layer. The titanium sample is anodized at up to 20 V in 1 M $(NH_4)_2SO_4$ + 0.5 wt% NH_4F [53]; (b) Smooth TiO_2 nanotubes 7 μm long produced in the glycerol electrolyte with 0.5 wt% NH_4F. The inset shows the walls of the nanotubes in more details [54]; (c) FE-SEM images of a nanotube array sample grown at 60 V in 0.25 wt% NH_4F in ethylene glycol [55]; (d) SEM images showing samples with double walls after annealing at 500 °C [56]; (e) cross-sectional image of an open bamboo structure [57]; (f) top SEM images of anodic oxide nanotubes formed on the Ti29Nb13Ta4.6Zr alloy (β type) and the inset shows its bottom [59].

diameter larger than 50 nm, resulting in dramatically reduced cellular activity and a high degree of programmed cell death, as shown in Fig. 16. Park et al. [63] have also researched the nanoscale response of two main bone cells (osteoblasts and osteoclasts) in an effort to explore whether (1) the nanotopography of cell interactions has a universal nature and (2) the balance between bone formation and bone resorbing cells can be influenced by a nanoscale topography. The results confirm that the nanotube surface topography largely affects bone cell differentiation involving osteoclastic activation and bone forming activity, indicating that 15 nm is a universal geometric constant for surface topography supporting cell adhesion and differentiation, as shown in Fig. 17.

Oh et al. [64] have investigated osteoblast cell growth on aligned TiO_2 nanotubes. The results obtained from their work indicate that the adhesion/propagation of osteoblasts is substantially improved by the topography of the TiO_2 nanotubes as manifested by the filopodia of growing cells actually going into the nanotube pores and producing an interlocked cell structure. The nanotube structure accelerates the growth of osteoblasts by as much as ~300–400%, as shown in Fig. 18. Moreover, TiO_2 nanotubes are considered as a drug release platform because of the open volume and excellent biocompatibility. However, when the drug is simply filled into a porous network or tubes, the main problem is the uncontrolled release of drugs or therapeutics. Controlled release kinetics is key to many novel drug delivery approaches and over the past few years, new structures, surface modification, and release principles have been widely explored. Hydrophobic surface modification is typically used to avoid undesired nonspecific adsorption of critical proteins (e.g., bovine serum albumin) to the drug delivery device [65]. Therefore, amphiphilic structures have attracted considerable attention because they combine a hydrophilic drug with a hydrophobic surface.

Song et al. [66] have fabricated amphiphilic TiO_2 nanotubes using a double anodization procedure combined with organic monolayer grafting and demonstrated that the amphiphilic TiO_2 nanotubular structure renders a highly controllable drug release system based on a hydrophobic cap on a hydrophilic TiO_2 nanotube. The hydrophobicity prevents uncontrolled leaching of

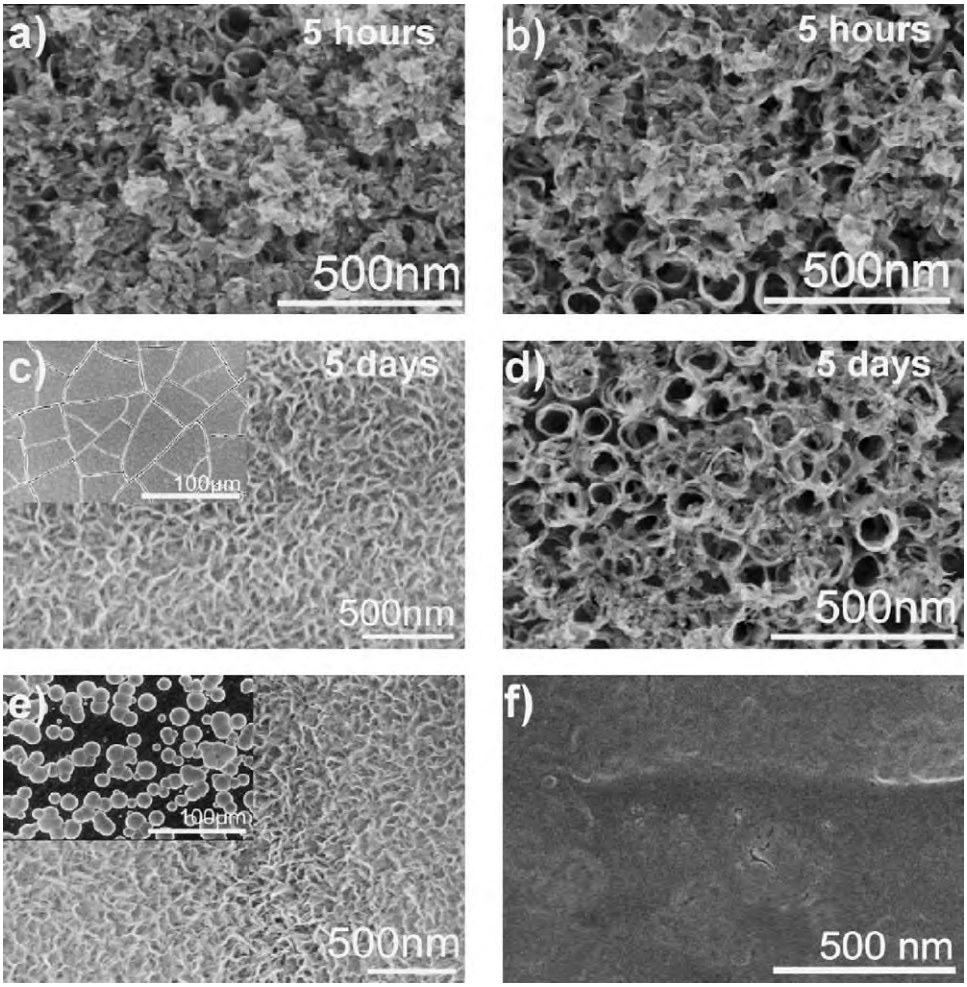

Fig. 15. SEM micrographs of annealed (a and c) and unannealed TiO_2 nanotubes (b and d) after exposure to SBF for (a and b) 5 h and (c and d) 5 days and annealed and unannealed compact TiO_2 layers after 5 days exposure to SBF (e and f). The insets show the respective layers at lower magnification [61].

hydrophilic drugs into an aqueous environment. By utilizing the photocatalytic nature of TiO_2 in UV induced chain scission of attached organic monolayers, the cap is removed and highly controlled release of drugs is achieved. Fig. 19 schematically describes the procedures associated with the fabrication of amphiphilic TiO_2 nanotubes (Fig. 19A) and drug loading approaches (Fig. 19B) reported by Song et al. To produce the amphiphilic tubes, the procedures consist of an initial anodization step forming tubes followed by hydrophobic surface modification. A second neat (hydrophilic) tube layer is grown underneath the first one by a second anodization process. The second layer consists of 2 μm long tubes (Fig. 19B) with a diameter of ~90 nm (inset of Fig. 20A). It is also clear that the second anodization process penetrates the bottom of the tubes grown during the first anodization step, and so tube growth (Fig. 20C and D) is reestablished as indicated by the field-induced breakdown of the monolayer occurring only at the tube bottom. After growth is re-established, the length of the tubes underneath can be controlled simply by the anodization time.

Yao et al. [67] have reported that anodized titanium possessing nanotubular surface structures (80 nm inner diameter and 200 nm deep) can be applied to drug delivery applications. To achieve local drug delivery, the anodized titanium with nanotubular structures are loaded with penicillin-based antibiotics using a co-precipitation method in which drug molecules are mixed in the simulated body fluid to collectively precipitate calcium phosphate crystals. Such co-precipitated coatings on the anodized nanotubular titanium can release drug molecules for up to 3 weeks. In addition, similar osteoblast adhesion is observed on the non-drug loaded and drug loaded precipitated calcium phosphate coatings on anodized titanium. Therefore, although anodized titanium can potentially be used in local drug delivery in orthopedic applications, it is necessary to investigate various issues systematically before clinical applications can be realized.

5.3. Micro-arc oxidation (MAO)

Micro-arc oxidation is also called anodic spark oxidation or plasma electrolytic oxidation (PEO). It is a relatively new anodic oxidation technique to deposit ceramic coatings on the surface of valve metals such as Al, Ti, Mg, Ta, W, Zn, and Zr and their alloys. Such metals in their natural state are protected by thin, self-healing, tightly adherent dielectric oxide films which resist the passage of current in the anodic direction. The current–voltage diagram pertaining to the MAO process is shown in Fig. 21. At relatively low voltages, the kinetics of the electrode processes for both systems obeys Faraday's law and the current–voltage characteristics of the cell vary according to Ohm's law. However, beyond a certain critical voltage, sparks and micro arc discharges occur and the behavior of a particular system may change significantly. MAO is thus a complex plasma-enhanced physico-chemical process incorporating micro-arc discharge, diffusion, plasma chemical reactions, and cataphoretic effects [68].

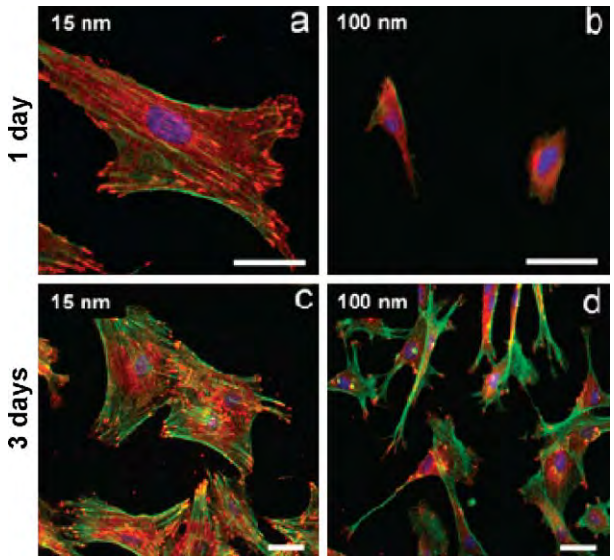

Fig. 16. Fluorescent images of focal contact formation of mesenchymal stem cells on 15 and 100 nm nanotubes. After 1 and 3 days of plating, focal contact formation and stress fiber assembly are extensive on the 15 nm nanotubes (a and c) as shown by anti paxillin staining (a–d red) and anti-actin staining (green), but strongly reduced on the 100 nm nanotubes (b and d). At day 3, (c) the cells are well spread on the 15 nm tubes, but (d) they develop a migratory morphology on the 100 nm tubes with few focal contacts and stress fibers (d). Blue: DAPI for nuclear staining. Bars: (a and b) 50 μm; (c and d) 100 μm [62]. (For interpretation of the references to color in this figure legend, the reader is referred to the web version of the article.)

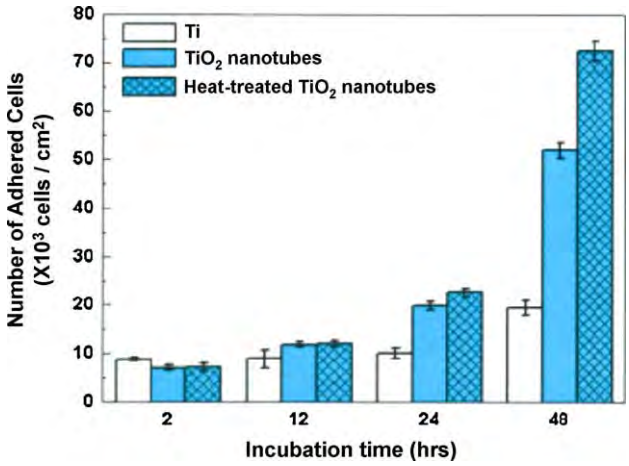

Fig. 18. Number of adhered cells as a function of incubation period on the surface of Ti, amorphous TiO_2 nanotubes and heated (anatase) TiO_2 nanotubes. The error bars in the figure represent the standard deviation for six samples for each data [64].

In MAO, the anode made by valve metals is immersed in an aqueous solution and an asymmetric alternating voltage is applied between the anode and cathode. In the anodic half circle, the voltage is usually in the range of 150–1000 V, whereas in the cathodic half circle, the voltage is in the range of 0–100 V. MAO processes are initiated by electrical discharge at the anode in the aqueous solution. A temperature of up to 10,000 K and local pressure of several hundred bars in the discharge channels have been reported. Using this technique, high quality coatings with high micro-hardness, adhesion, strength, and wear resistance can be synthesized. The quality of the MAO coating is determined by parameters such as the electrolyte composition, electrolyte temperature, alloy composition, voltage, current density, time, and so on, and high quality coatings can be produced by using optimized deposition parameters.

The formation mechanism in MAO ensures the following characteristics of the resulting films and coatings: (a) firm adhesion to substrates [69], (b) porous structure, (c) nanostructure, and (d) tolerance on samples with different geometric shapes. The typical SEM and TEM photographs of the MAO coatings on Ti, Zr and titanium alloys are shown in Fig. 22. It is clear that the coatings are porous and the pores are homogenously distributed on the coatings surface. The size of the surface grains observed by FE-SEM is about 10–50 nm (Fig. 22a and b). TEM observation shows that the size of the grains in the coating is about 10–50 nm, indicating that coatings produced by MAO are nanostructured (Fig. 22c). The selected area electron diffraction (SAED) pattern acquired from point A in Fig. 22c suggests that the structure is polycrystalline.

MAO coatings have been extensively investigated due to their superior corrosion resistance [73], thermal stability [74], photocatalytic activity [75], wear resistance [76] and CO sensing properties [77]. Since Ishizawa et al. [78] first applied the technique to biomedical titanium implants, it has gained much attention from the biomedical community. Song et al. [79] reported biomimetic deposition of apatite on Ca and P-containing MAO coatings. Zhao et al. [80] investigated the osteoblast behavior on the surface of MAO coatings. The MAO coatings benefit osteoblast adhesion and the ALP activity of osteoblast cells on

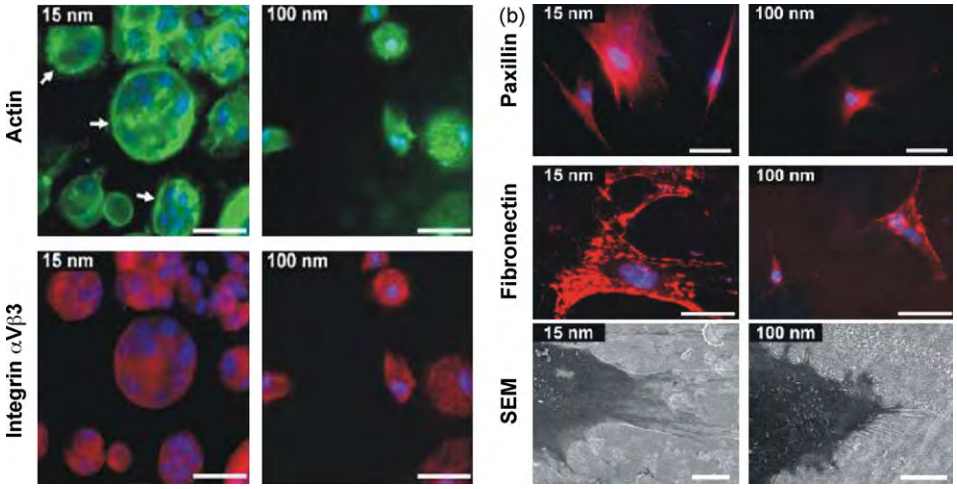

Fig. 17. (a) Cell morphology reveals large osteoclasts only on the 15-nm nanotubes. Scale bars: 50, 200, and 200 μm; (b) size-dependent response of primary human osteoblasts to TiO_2 nanotubes. SEM image shows that development of focal contacts measured by paxillin staining (upper panel) (scale bars: 100 μm), extracellular deposition of fibronection matrix (middle panel) (scale bars: 50 μm), and filopodia formation (lower panel) are highest on the 15 nm nanoubes (scale bars: 10 μm) [63].

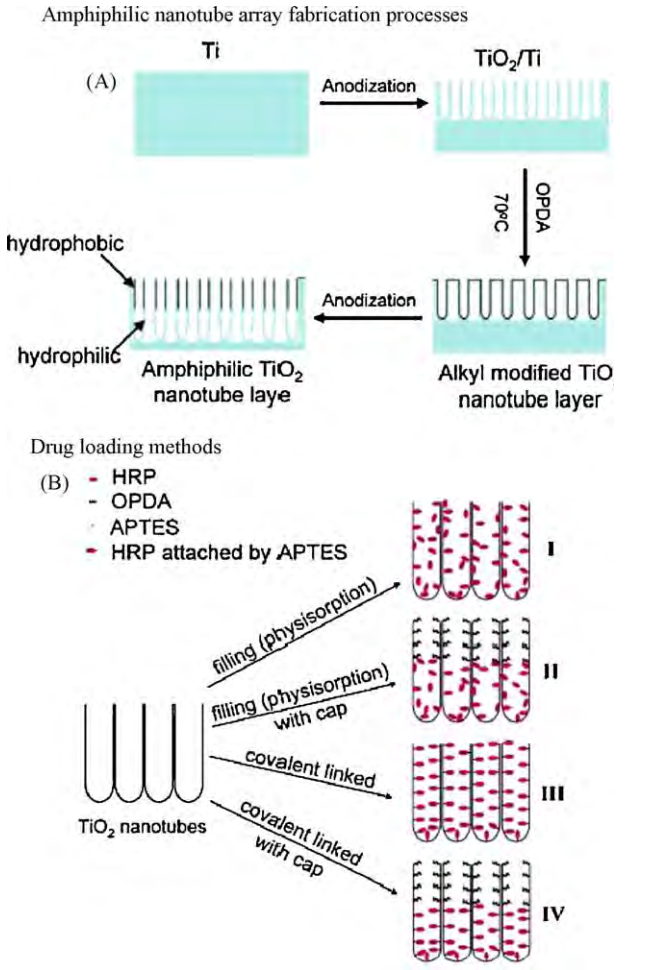

Fig. 19. (A) Schematic of the procedures to fabricate amphiphilic TiO_2 nanotube layers, and (B) four methods for drug loading using horseradish peroxide (HRP) as a hydrophilic model drug: (I) immersion without any TiO_2 surface modification (for reference), (II) immersion after OPDA modification in the upper nanotube layer (hydrophobic cap), (III) covalently attached HRP over the entire nanotube layers, and (IV) OPDA cap in the upper nanotube layer and covalently attached HRP to the lower nanotube layer [66].

the MAO coatings is higher than that on polished and sand blasted surfaces. *In vivo* tests in rabbits show considerable improvement in the osseo-integration capability compared to pure titanium implants [81,82]. By coupling with other techniques such as UV irradiation, chemical treatment, and electron beam evaporation, MAO coatings with improved biological performance can be obtained [70,83,84].

By tailoring the electrolyte composition, different kinds of nanostructured composite coatings with variable functions can be prepared [85–87]. Mg, Zr, Al, and their alloys after MAO have been used as nanostructured coatings in biomedical applications and some positive *in vitro* results have been reported [71,88]. For instance, MAO modification has been performed on zirconium to produce macroporous and nano-crystalline zirconia films and the effects of chemical treatment in aqueous H_2SO_4 or NaOH solutions on the microstructure and apatite formation ability on the films have been investigated by Han et al. [89]. It is believed that the enhanced apatite forming ability rendered by the chemically treated ZrO_2 films is related to the abundant basic Zr–OH groups on their surface.

In summary, MAO is a promising method to prepare nanostructured films and coatings on Ti, Mg, Zr, Al, and their alloys. Biometals with nanostructured surfaces treated by MAO have potential applications in orthopedic and dental implant materials.

5.4. Sol–gel

The sol–gel process is widely used to deposit thin ceramic coatings (<10 μm). Compared to conventional thin film processes, this technique allows for better control of the chemical composition and microstructure of the coating, preparation of homogeneous films, reduction of the densification temperature, and last but not least, simpler equipment and lower cost. It is especially easy to purify the precursors by distillation or crystallization and to take the opposite approach to introduce trace elements. In addition, these precursors can be mixed at the molecular level in the solution and a high degree of film homogeneity can be attained. This process thus permits lower processing temperature during sintering.

The sol–gel process can be divided into five main steps [90]: (1) hydrolysis and polycondensation, (2) gelation, (3) aging, (4) drying, and (5) sintering. Sol–gel derived coatings are usually produced using the spin coating or dip coating techniques. The spin coating process consists of four stages: deposition, spin up, spin off, and evaporation. For complex shaped substrates, the commonly used sol–gel technique is dip coating. The dip coating consists of three steps, dipping, withdrawal, and heating. In dip coating, a substrate is dipped in a homogeneous sol solution containing various metal compounds which finally form the desired simple or complex oxides. A liquid film on the substrate becomes a gel film upon withdrawal of substrate from the solution as a result of the gelation process [91]. Finally, the substrate with a gel film is heated to a certain temperature to produce chemical bonding between the film and substrate [92].

The resulting microstructure in the sol–gel coating depends on the precursors as well as relative rates of condensation and evaporation during film deposition and it is quite straightforward to synthesize nanostructured coatings. For instance, Advincula et al. [93] have prepared titanium oxide films on Ti-6Al-4V substrate using the sol–gel process and the coating is composed of amorphous titanium oxide with nanopores (5–50 nm) and micropores. He et al. [94] have produced nano-TiO_2/HA composite coatings on titanium disks using the sol–gel method. The anatase coating which adheres strongly to the titanium substrate serves as the inner layer and the porous HA coating which has a higher solubility and better short-term bioactivity is used as the outer layer. Such a nano-TiO_2/HA composite coating exhibits good crystallization, homogeneity, and adhesion (Fig. 23). Peltola et al. [95] investigate the apatite forming ability of different kinds of sol–gel derived titania coatings on commercial titanium and reported that the best apatite forming ability is achieved by the addition of valeric acid to the sol (600 °C) or sintering of the sol–gel coating at 450–550 °C. Jokinen et al. [96] evaluate the influence of the sol and surface properties on the bioactivity of titania and titania–silica films *in vitro*. All the titania films show good bioactivity, but the titania–silica films do not. Moreover, titania films with the smallest particle size and narrow particle size distribution show hydroxyapatite precipitation later than the other titania films. The difference in the precipitation behavior may be attributed to the different surface characteristics, although bulk properties such as porosity and film thickness do not show apparent influence on the bioactivity. In generally, apatite precipitation occurs on the titania films when the following factors are favorable to the adsorption of cations and formation of an electric double layer, namely surface topography, charge, charge density, and high affinity of ions allowing adsorption onto the surface rather than staying in the solution. In addition, in order to obtain a bioactive surface, the particle size in the sol must not be too small or the particles should have aggregated structures in order to produce an uneven surface.

The bioactivity of nano-titania thin films prepared by layer-by-layer assembly has been investigated by Dinesh et al. [97]. Larger

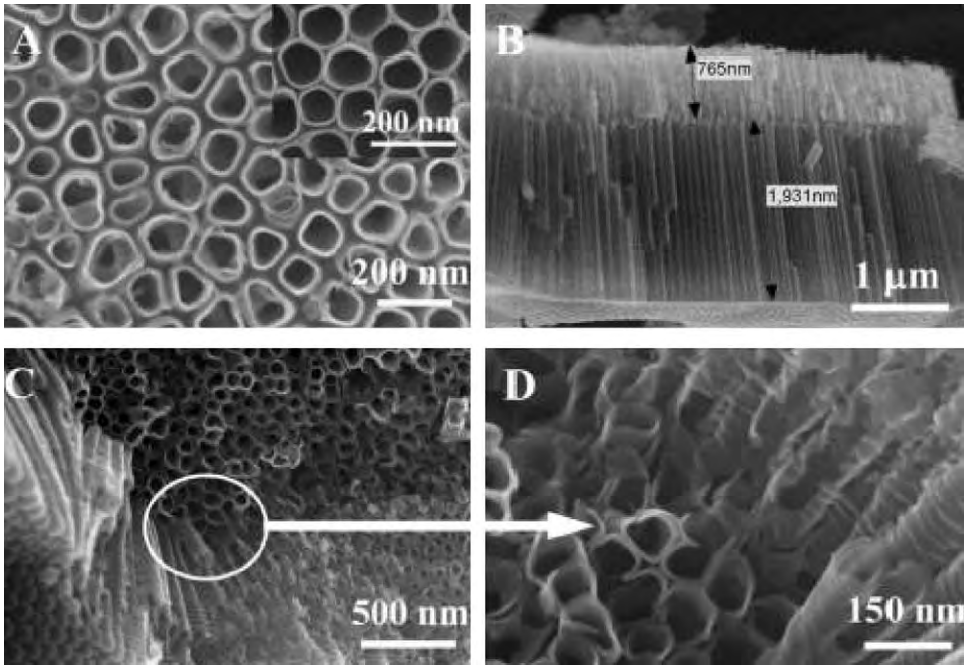

Fig. 20. (A) SEM top-view images of the first nanotube layer and the second nanotube layer (inset of A), (B) cross-sectional image of the double nanotube layers, and (C and D) cross-sectional images of the interface between the upper and lower TiO_2 nanotube layers [66].

surface roughness is observed with increasing number of layer-by-layer assembled TiO_2 thin films. Cultured mouse mesechymal stem cells exhibit no cytotoxic effects on the TiO_2 coated substrates. Proliferation and attachment of MSCs increase after deposition of TiO_2 nanoparticle layers and a higher number of cells are attached if the number of layers of TiO_2 nanoparticle thin films increases. Spreading of cells is also faster on surfaces with a larger number of layers of TiO_2 nanoparticles suggesting enhanced attachment and faster spreading of cells on rougher surfaces. Liu et al. [98] have deposited 205 nm thick TiO_2 films embedded with nm-scale TiO_2 particles on NiTi alloy using the sol–gel method to enhance the biocompatibility. The films which are mainly anatase are compact and smooth. *In vitro* blood compatibility determined by the dynamic clotting time and blood platelets adhesion tests show that NiTi alloy coated with TiO_2 possesses improved blood compatibility. Eisenbarth et al. [99] have investigated the interactions between osteoblast-like MC3T3-E1 cells and Nb_2O_5 sol–gel coatings on cp-titanium. Clear coherence of migration, adhesion, and collagen I production processes are observed from the surface structure and it is observed that the smoother the surface, the faster are cell migration and adhesion. The intermediate roughness (R_a = 15 nm) results in a slower adhesion and migration but overall stronger cell adhesion, as evidenced by the spreading area and the actin cytoskeleton distribution in the cells. The rather rough and hilly surface with R_a = 40 nm slows migration but leads to appropriate spreading and cell adhesion on the surface.

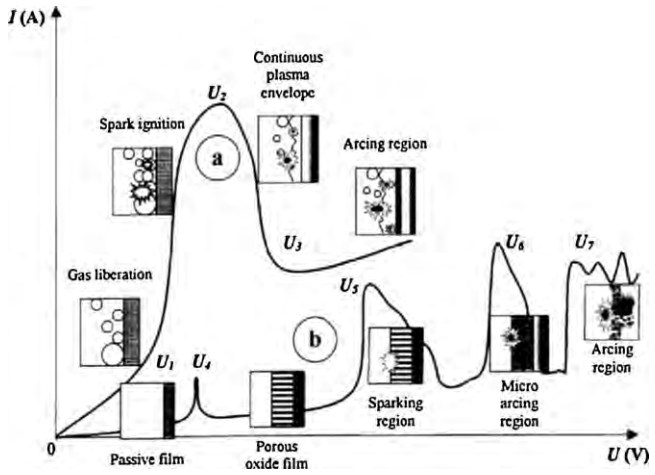

Fig. 21. Two kinds of current–voltage diagram for the processes of MAO: discharge phenomena are developed (a) in the near-electrode area and (b) in the dielectric film on the electrode surface [68].

5.5. Plasma spraying

Plasma spraying is widely used to prepare ceramic coatings since its advent in Union Carbide in the mid-1950s. During plasma spraying, the temperature in the core region of plasma beam is relatively constant at approximately 12,000 K and almost all materials can be melted in the plasma jet. In fact, plasma spraying is a rapid heating/cooling solidification process. The cooling rate of the molten or partially molten droplets is in excess of 10^6 K/s and it is possible to introduce nanoscale properties to plasma sprayed coatings.

Nanostructured zirconia coatings have been prepared by plasma spraying [100–104]. The nanostructured zirconia coatings possess two kinds of structure, namely the main structure composed of loose nanosized particles and a secondary overlapping structure consisting of micrometer size particles. The zirconia coating has the same phase composition as the starting powders and the thickness of the coating is quite uniform. However, the thickness of the zirconia coating appears to be inconsistent as revealed by cross-sectional micrographs and more work has been conducted to further investigate the preparation and properties of plasma-sprayed nanostructured zirconia coatings. Zirconia coatings with a nanostructured surface and uniform thickness have been successfully fabricated by optimizing the spraying parameters, as shown in Fig. 24.

Plasma sprayed nanostructured zirconia coatings stabilized with 3 mol% yttria (3Y-TZP) also exhibit some bioactivity. After immersion in the SBF solution for 28 days, bone-like apatite is formed on the surface of the nanostructured zirconia coatings. On the other hand, no apatite is formed on the surface of the polished

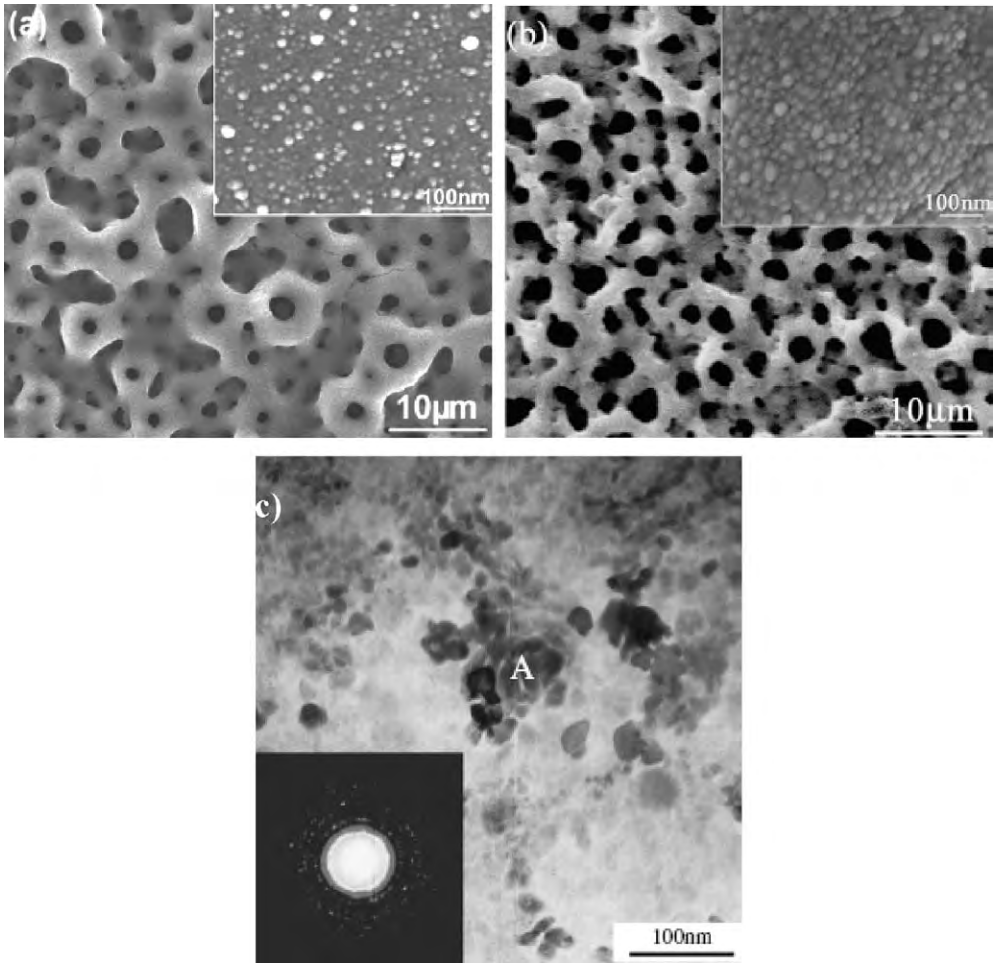

Fig. 22. Surface morphologies of the MAO coatings on (a) titanium [70] and (b) zirconium [71]; (c) TEM micrograph of MAO coating formed on Ti6Al4V alloy [72].

coating. Therefore, the nanostructured surface of the plasma sprayed 3Y-TZP coating is believed to be the key to its bioactivity.

Commercially available nanometer-sized TiO_2 powders with size of about 30 nm made into sphere-like particles of 45–90 μm using a spray drying process have been deposited onto Ti-6Al-4V substrates by atmospheric plasma spraying under modified spraying parameters [105]. The surface SEM views of the as-sprayed TiO_2 coatings displayed in Fig. 25 indicate that the surface of the nano-TiO_2 coating comprises particles about 50 nm in size (Fig. 25b). The cross-sectional TEM views reveal that the thickness of the outer layer with nano-sized particles is about 500 nm, as shown in Fig. 26. In the interior of the coating, most of the grains possess a columnar morphology with a diameter of about 100–200 nm. The difference in the crystal growth between the surface and interior of the coating depends mostly on their thermal history. During plasma spraying, the bulk of the coating tends to give rise to larger columnar grains due to the continuous heat provided by the plasma and subsequent melt, whereas the surface grains are subjected to less heating. After immersion in SBF for 28 days, the surface of the hydrogen implanted and UV-illuminated nano-TiO_2 coating is completely covered by bone-like apatite. In contrast, in the control experiments involving the as-sprayed nano-TiO_2, conventional-TiO_2 coatings, hydrogen implanted or UV-illuminated conventional-TiO_2 coating, hydrogen implanted, or UV-illuminated polished nano-TiO_2 coating on which the nanostructured surface has been removed, no apatite can be observed on the surface after soaking in SBF for 28 days [105–107]. The results indicate that only the hydrogen implanted and UV-illuminated nano-TiO_2 coatings with nanostructured surfaces can induce the formation bone-like apatite. It can thus be inferred that the bioactivity of plasma-sprayed TiO_2 coatings depends on the nanostructured surface composed of enough small particles and hydrogen incorporation or UV-illumination. The *in vivo* results also prove that the as-sprayed nano-TiO_2 coatings do not induce the formation of new bones during the implantation period, but the UV-irradiated nano-TiO_2 coatings prompt the formation of new bone on the surface after implantation for longer than 2 months (Fig. 27) [107]. The difference in the new bone formability between the two coatings may be due to the different surface characteristics. *In vitro* tests indicate that apatite can nucleate on the surface of the nano-TiO_2 coatings after UV irradiation in SBF for longer than 12 h. It is well known that bioactive implants have better bone conductivity than bioinert implants and so it is reasonable that new bones can grow on the UV-irradiated nano-TiO_2 coatings but not on the as-sprayed nano-TiO_2 coatings under *in vivo* conditions.

The results obtained from the nano-TiO_2 coatings indicate that the nano-sized surface bodes well for bioactivity and biocompatibility compared to a conventional surface. Deposition of calcium ions is the first and most crucial step of carbonate-containing hydroxyapatite nucleation from an ionic solution. This process is believed to initiate the growth of bone-like apatite on the surface of biocompatible implants [108]. Formation of a negatively-charged surface gives rise to apatite precipitation because positive calcium ions are attracted from the solution [109] and the charge densities of the particles are determined by its size. Vayssieres et al. [110] suggest that finer nanocrystalline particles have higher surface

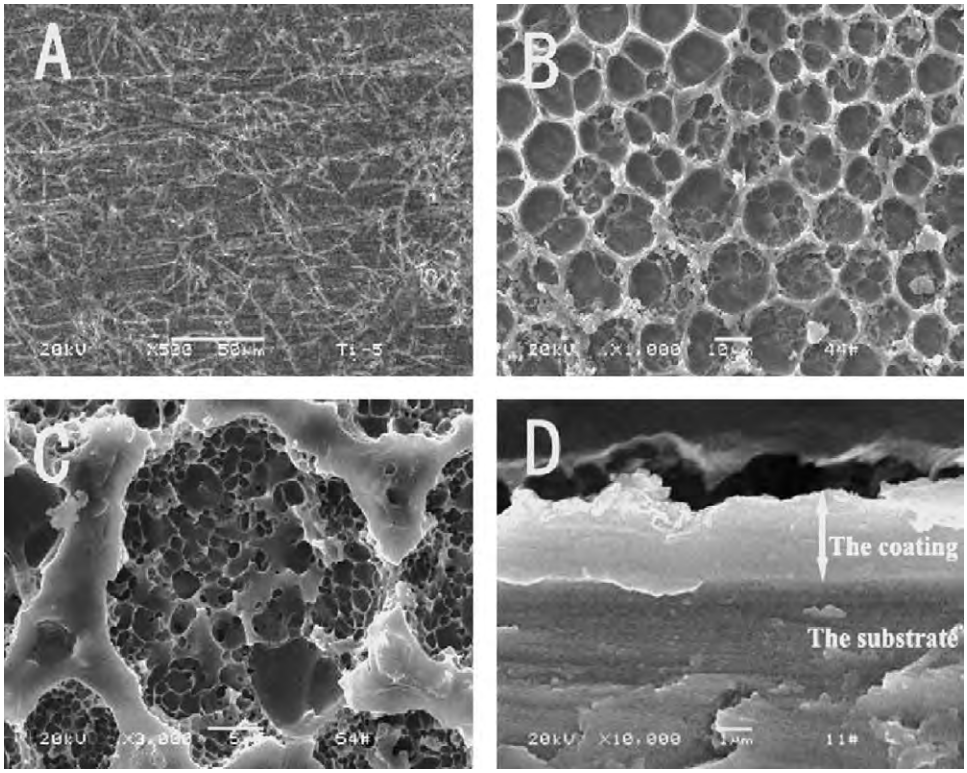

Fig. 23. SEM images of the coatings: (A) surface of the conventional HA coating, 500×; (B and C) surface of the TiO_2/HA composite coating, 1000×, 3000×; (D) Cross section view of the TiO_2/HA composite coating, 10,000× [94].

charge densities than larger ones. Thermodynamic analysis reveals that the surface or interfacial tension diminishes with decreasing particle size as a result of the increased potential energy of the bulk atoms in the particles [111]. Smaller particles with increased molar free energy are more likely to adsorb molecules or ions onto their surfaces in order to decrease the total free energy and to become more stable. Therefore, these nano-sized particles in the outermost layer of the TiO_2 coating may be the key factor inducing the precipitation of bone-like apatite on the surface during immersion in SBF.

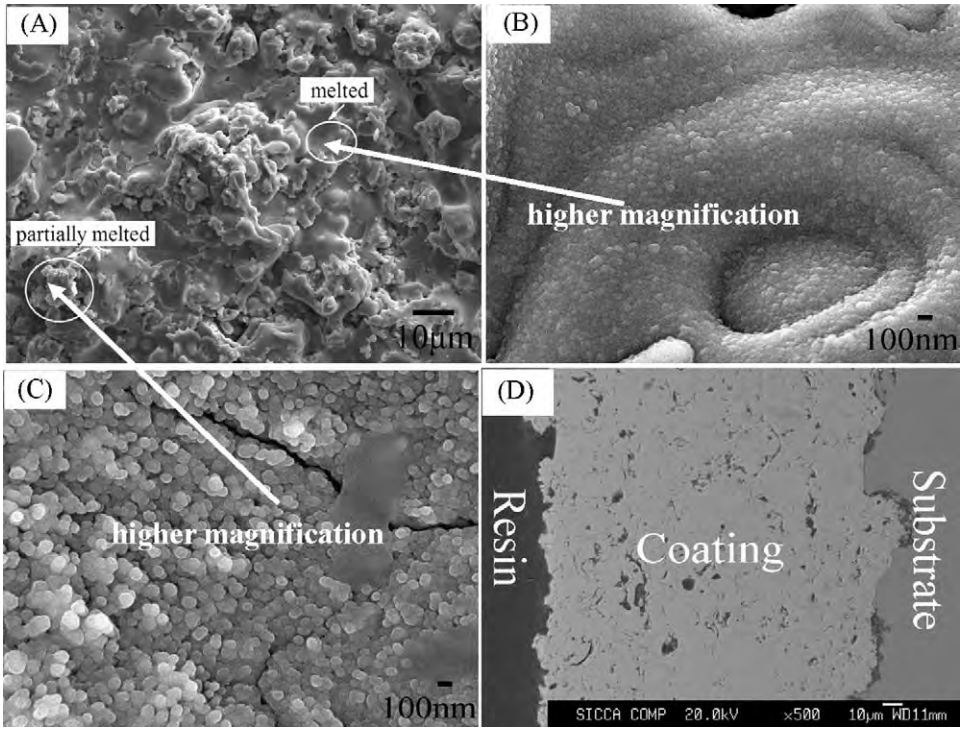

Fig. 24. (A–C) Surface and (D) cross-section views of the as-sprayed nanostructured 3Y-TZP coatings [104].

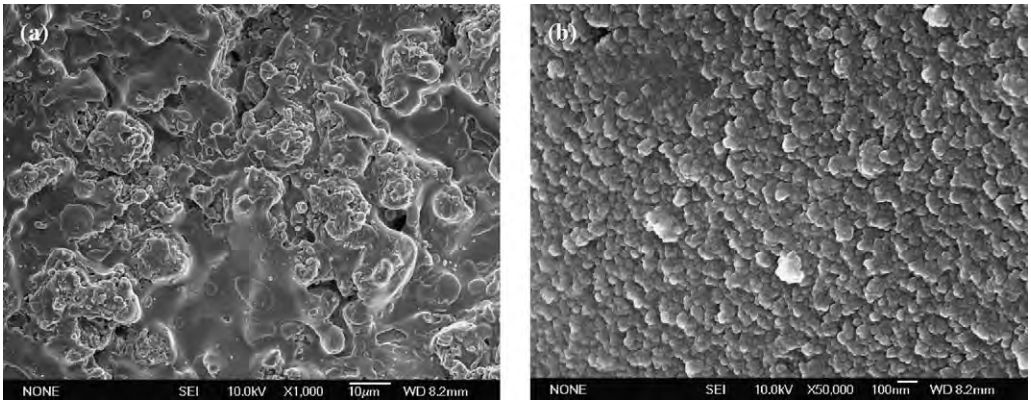

Fig. 25. Surface SEM views of as-sprayed nano-TiO_2 coating: (a) 1000× and (b) 50,000× [105].

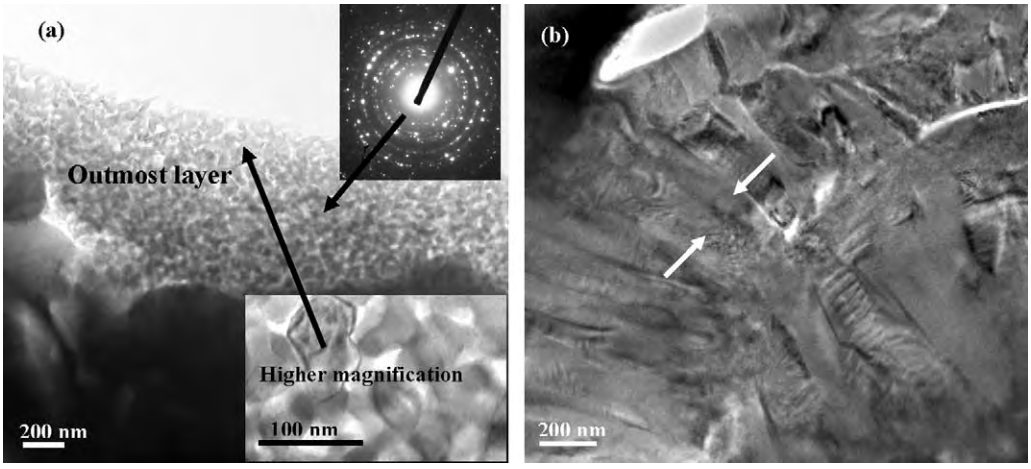

Fig. 26. Cross-sectional TEM views of the as-sprayed nano-TiO_2 coating: (a) coating surface and (b) coating interior [105].

5.6. Surface mechanical attrition treatment

Surface mechanical attrition treatment has been proven to be an effective approach to obtain a hard layer due to the formation of a nanocrystalline structure in the surface layer of a metal. The basic principle of SMAT is the generation of plastic deformation in the top surface layer of a metal by means of repeated multidirectional impacts of flying balls on the sample surface. Plastic deformation of the surface layer with a large strain and high strain rate results in progressive refinement of coarse grains into the nanometer regime. The process is illustrated in Fig. 28a [112]. Stainless steel balls with a mirror-like surface are placed at the bottom of a cylinder-shaped vacuum chamber attached to a vibration generator. Because of the high vibration frequency of the system, the sample surface under treatment was struck repetitively by a large number of balls within a short period of time, resulting severe plastic deformation in the near surface (Fig. 28b). As a consequence, grains in the surface layer are effectively refined into the nanometer scale. As reported in many papers concerning SMAT, there are actually two factors governing the grain refining process: stacking fault energy (SFE) and the number of slip systems in the metals.

As SMAT is simple, flexible, and economical, it is potentially useful in industrial applications. The technique has in fact been applied to a number of metals such as aluminum [113], iron [114,115], and stainless steel [116,117]. Another advantage of surface nanocrystallization is that it greatly enhances the diffusion kinetics of atoms. It has been found that the nitriding temperature of iron produced using SMAT can be reduced to 300 °C, which is at least 200 °C below the conventional nitriding temperature [112]. It has been demonstrated that commercial pure titanium with an ultrafine grain structure in the nanometer range can be processed using severe plastic deformation methods such as equal channel angular pressing (ECAP) [118] and high pressure torsion (HPT) [119]. These processes nearly triple the strength of pure titanium and it can have a profound impact on applications. SMAT can also be employed to produce a nanostructured surface on titanium to improve the surface properties.

Zhu et al. [120] have reported that a nanostructured surface layer up to 50 μm thick can be produced on commercial pure titanium using SMAT and investigated the formation mechanism of the nanostructured surface. It is thought that the grain refinement process accompanied by an increase in the strain in the surface layer involves: (1) onset of twins and intersection of twin systems, (2) formation of dislocation walls, (3) nucleation of microbands associated with the splitting of dislocation walls, (4) subdivision of microbands into low angle disoriented blocks and then highly disoriented polygonal submicronic grains, and (5) further breakdown of submicronic polygonal grains into randomly oriented nanograins. At the same time, Guo et al. [121] in same group investigate the thermal properties of ultrafine-grained pure titanium surface layer produced by SMAT. The nanostructured surface obtained by SMAT has different thermal conductivity which depends strongly on the grain size. Compared to the coarse-grain matrix in the SMAT treated-titanium, the thermal conductivity of the nanostructured surface layer decreases substantially.

Wen et al. [122,123] have investigated the formation of nanoporous titania on bulk titanium by hybrid SMAT. In this process, a commercial Ti plate first undergoes SMAT in vacuum for 1 h and then is immersed in 30 wt.% H_2O_2 for 24 and 48 h at room

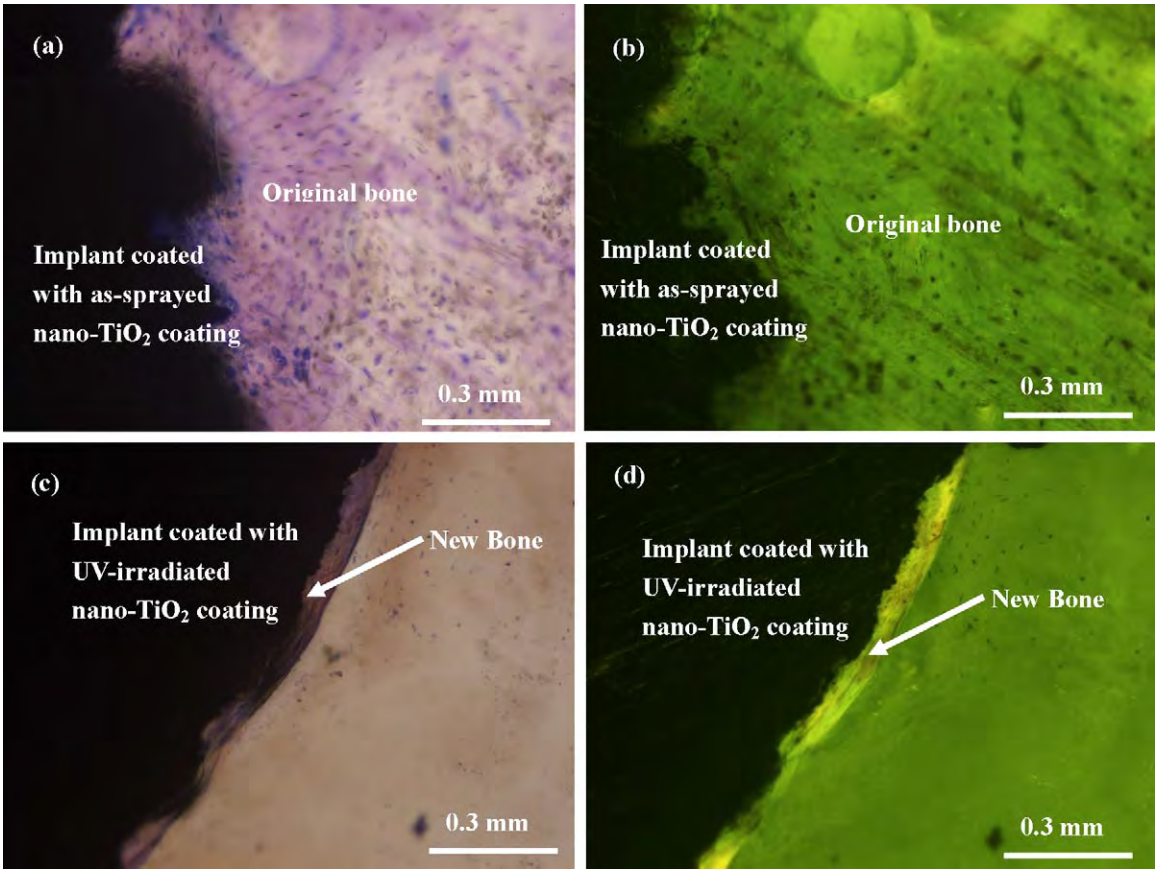

Fig. 27. Histological morphology of the cross-section of the (a and b) as-sprayed and (c and d) UV-irradiated nano-TiO_2 coating after implantation in the medial femoral condylus of rabbits for 2 months: (a and c) un-decalcified section stained by toluidine blue, (b and d) fluorescence view of the un-decalcified section marked by tetracycline [107]. (For interpretation of the references to color in this figure legend, the reader is referred to the web version of the article.)

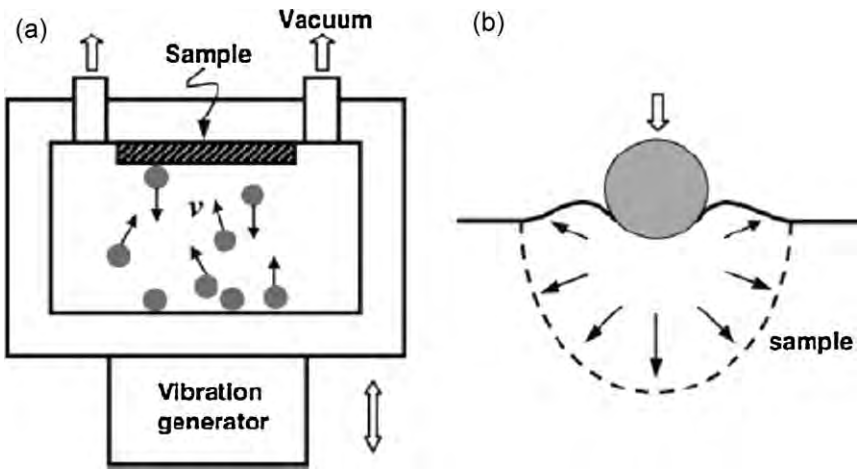

Fig. 28. (a) Schematic illustration of the SMAT technique and (b) localized plastic deformation zone induced by the vibrating ball [112].

temperature. A gradient Ti surface as shown in Fig. 29 is formed. The SMAT Ti shows much improved oxidation kinetics in the H_2O_2 solution compared to coarse grain Ti. The hybrid SMAT method produces nanoporous titania on bulk Ti via *in situ* synthesis, and the nanoporous structure can be retained even after calcination at 600 °C, indicating the thermal stability as shown in Fig. 30. Formation of the nanoporous structure on the SMAT Ti surface is attributed to quick H_2O_2 decomposition, preferred oxidation of nanocrystalline Ti with dense defects to form amorphous titania, and *in situ* crystallization and dissolution of titania gel. The SMAT method can thus be used to improve the bioactivity of titanium bone implants and to accelerate osseointegration. Wen et al. [124] have also investigated the tensile properties of SMAT Ti and found that the nanocrystalline Ti made by SMAT has high strength. The low deformation temperature and high strain rates suppress dynamic recovery in SMAT thereby facilitating grain refinement of Ti (~30 nm). At the same time, the depressed strain hardening of nanocrystalline Ti can be attributed to the small grain size with nearly saturated dislocation density. On the contrary, bulk SMAT Ti shows good mechanical properties which combine strengthening from nanocrystalline Ti along with strain hardening provided by dislocation activity in coarse grain Ti.

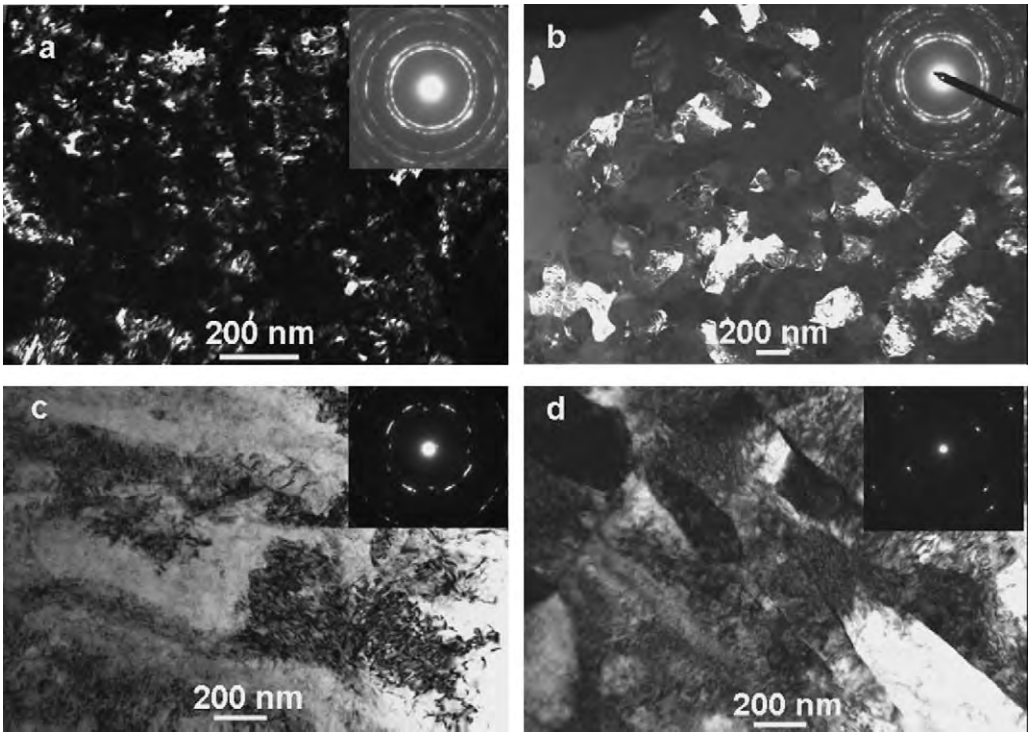

Fig. 29. Typical plane-view TEM observations and corresponding SAED of the (a) top-surface, (b) sub-surface layer of 60 mm depth, (c) sub-surface layer at 100 mm depth, and (d) sub-surface layer of 150 mm depth in the SMAT Ti [122].

Zirconium (Zr) has been studied as biomaterials. As a simple hexagonal close packed (hcp) metal, Zr has moderate SFE (about 80 mJ m^{-2}) which is higher than that of Co but lower than that of Ti. Zhang et al. [125] have investigated the structure evolution and grain refinement mechanism of Zr during SMAT. A nanostructural layer with thickness of about 20 μm is produced on commercial pure Zr using SMAT. In the initial stage of SMAT, twinning dominates plastic deformation of Zr and divides the coarse grains of Zr into finer twin plates. With increasing strain, intersection of twins occurs and dislocation slips are activated becoming the predominant deformation mode instead of twinning. As a result of the dislocation slips, high-density dislocation arrays are formed and they further subdivide the twin plates into subgrains. With further increase in the strain, the dislocations accumulate and rearrange to minimize the energy state of the high-strain-energy subgrains. The dense dislocation walls are converted to grain boundaries and the submicrometer grains are subdivided leading to the formation of nanosized grains at the top of the SMATed surface, as shown in Fig. 31.

According to published papers on SMAT applications to biomedical metals, many biological properties such as biocompatibility, bioactivity, interactions between nanostructured surface and cells, proteins and body fluids, as well as the further functionalization of biomedical metals after SMAT have not been studied in details. Therefore, it remains a relatively unexplored area and more work is needed before SMAT can be clinically useful.

5.7. Physical vapor deposition

Physical vapor deposition involves atomistic deposition processes in which materials are vaporized from a solid or liquid source in the form of atoms or molecules, transported in the form of a vapor or plasma in a vacuum or low pressure gaseous environment to the substrate where they condense [126]. Typically, PVD processes are employed to fabricate films with thicknesses ranging from a few nanometers to thousands of nanometers. The main PVD processes are evaporation, sputtering, vacuum arc deposition, ion plating, and ion implantation & deposition.

Evaporation is a PVD process in which materials from a thermal vaporization source reaches the substrate with little or no collision with gas molecules in the space between the source and substrate. The trajectory of the vaporized materials is "line-of-sight". The thermal sources for evaporation include resistance heating [127], electron beam [128], laser beam [129], and so on. Recently, matrix-assisted pulsed laser evaporation (MAPLE) has been shown to be a promising alternative to conventional pulsed laser deposition [130] for the fabrication of polymers and other organic thin films [131]. Besides, the matrix-assisted pulsed-laser evaporation direct-write (MAPLE DW) process allows for computer-controlled deposition [132] making it more convenient during film fabrication.

In sputtering, particles are vaporized from a target by some physical sputtering processes. Byrne et al. [133] have studied the protein adsorption behavior on magnetron sputtered Al-, Nb-, Ta- and Ti-containing thin films. According to the experimental results which indicate that Al (Al_2O_3) adsorbs less fibrinogen and albumin compared to Nb (Nb_2O_5), Ta (Ta_2O_5), and Ti(TiO_2), it is concluded that protein adsorption onto these films is closely correlated to the surface oxide fractions. Liu et al. [134] have evaluated the bacterial adhesion behavior on Si- and N-doped DLC coatings with surface roughness ranging from 33.381 nm to 57.709 nm prepared by magnetron sputtering. Bacterial adhesion decreases with increase work of adhesion and it is consistent with thermodynamic theories. Better blood compatibility is observed from La_2O_3 doped DLC films in comparison with pure DLC [135]. The stoichiometry and nanotopography (surface roughness) are found to affect platelets response to the TiNx thin films prepared by direct current reactive magnetron sputtering [136]. According to atomic force microscopy (AFM), stoichiometric and smoother TiN films promote platelets adhesion and activation compared to rougher nonstoichiometric $TiN_{x=1.1}$ films. A bioactive DLC film containing titanium dopant has been prepared by co-sputtering [137]. The enhanced cell attachment, proliferation, and differentiation on Ti doped DLC is believed

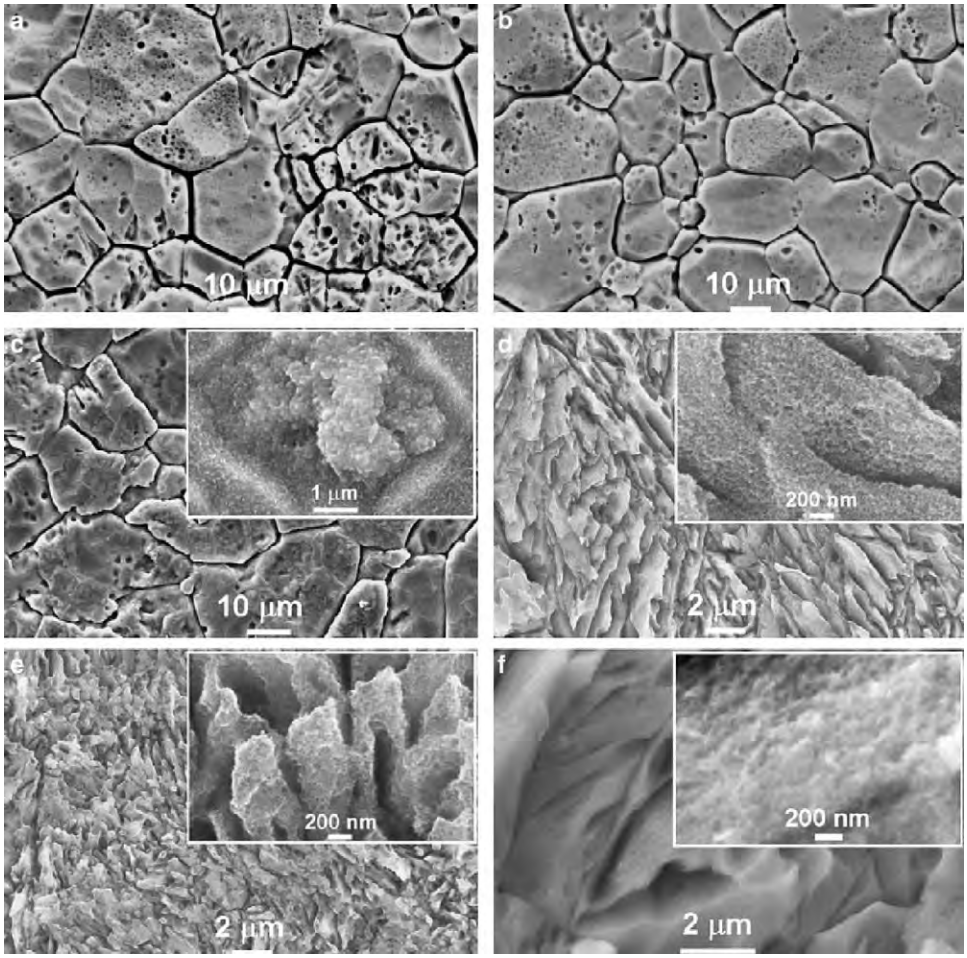

Fig. 30. SEM pictures of (a–c) coarse-grained Ti and (d–f) SMAT Ti top surface. (a) Coarse-grained Ti after oxidation at room temperature for 24 h; (b) postcalcination of (a) at 400 °C for 1 h; (c) post-calcination of (a) at 600 °C for 1 h; (d) SMAT Ti after oxidation at room temperature for 24 h; (e) post-calcination of (d) at 400 °C for 1 h; (f) post-calcination of (d) at 600 °C for 1 h [123].

to be related to the plasma energy during deposition which enhances densification of the film and consequently improves the surface contact area of the adsorbed proteins.

Vacuum arc deposition is a PVD process which utilizes vaporized materials emitted from an electrode under arcing conditions. Vacuum arc plasma deposited diamond-like carbon (DLC) films with nano scale thickness (up to several hundred nanometer) have good biocompatibility and are promising coatings in biomedical devices including orthopedic implants[138]. Recently, doped DLC films have attracted much attention. Silver (Ag) doped DLC films by pulsed filtered cathodic vacuum arc are potentially useful biomaterials having both good blood compatibility and antimicrobial properties [139]. However, the approach must be considered more generally because the altered electrical properties resulting from the

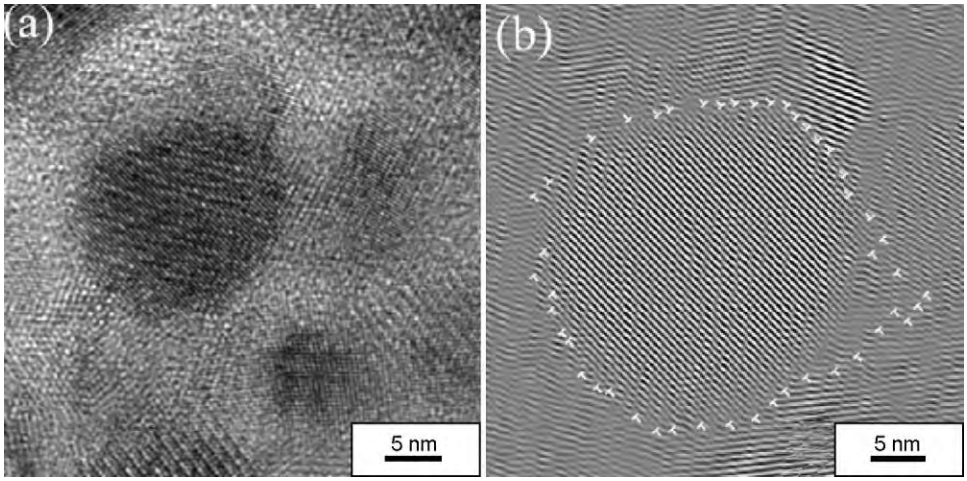

Fig. 31. (a) A high-resolution TEM image and (b) an inverse Fourier image of the top surface layer, showing nanograins of size about 10 nm and dislocations along the boundary, respectively [125].

doping processes may harm to physiochemical properties of the DLC coatings. According to Khun et al. [140], increase in the doped nitrogen content in the DLC films increases the electrical conductivity which in turn accelerates electron transfer kinetics and decreases the corrosion resistance of the DLC films.

SiO*x* films with many small island-like protuberances (10–70 nm) have been fabricated by pulsed metal vacuum arc deposition technology [141]. Apatite can form on the surface of the SiO*x* film after immersion in SBF because of the nanometer scale topography and oxygen vacancies galore in the film. Titanium oxide films with grains size of 80–100 nm deposited on Ti6Al4V substrates using pulsed metal vacuum arc deposition exhibit wear resistance that is approximately 10 times better than that of bare Ti6Al4 V [142]. Leng et al. [143] compare the blood compatibility of TiO_2 produced by pulsed vacuum arc plasma deposition and unbalanced magnetron sputtering. It is suggested that because of the grain size and roughness differences (130–160 nm for pulsed vacuum arc plasma deposition versus 170–230 nm for UBM sputtering), the platelet adhesion behavior on rutile TiO_2 synthesized by the UBM sputtering is better than that synthesized by pulsed vacuum arc deposition.

ZrO_2 thin films with nano-sized surface have been fabricated on n-type, 100 mm Si (1 0 0) wafers using a filtered cathodic arc system [144]. The experimental apparatus used in this study includes a magnetic duct and cathodic arc plasma source as depicted in Fig. 32. The surface views of the as-deposited and thermally treated ZrO_2 thin films observed by SEM and AFM are displayed in Figs. 33 and 34. The surface of the as-deposited ZrO_2 thin film is very smooth and the surface features cannot be distinguished very well by SEM, as shown in Fig. 33a. However, some very small particles can be observed on the surface of the as-deposited ZrO_2 thin film from the AFM picture (Fig. 34a). After the ZrO_2 thin film is annealed at 1000 °C for 2 h, the particles on its

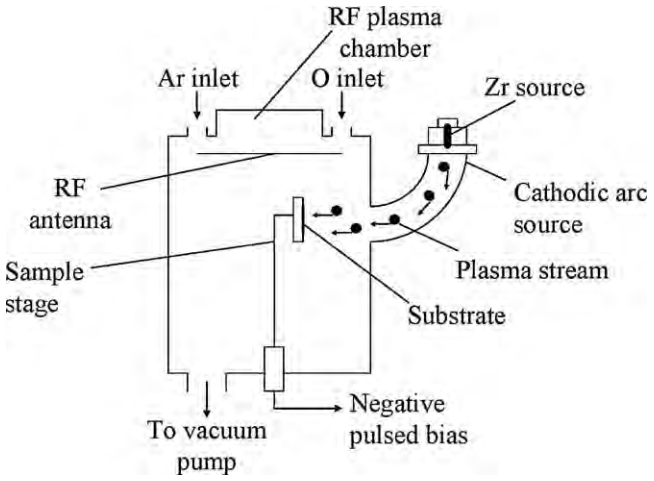

Fig. 32. Schematic diagram of the magnetic duct and cathodic arc plasma source used to prepare ZrO_2 samples [144].

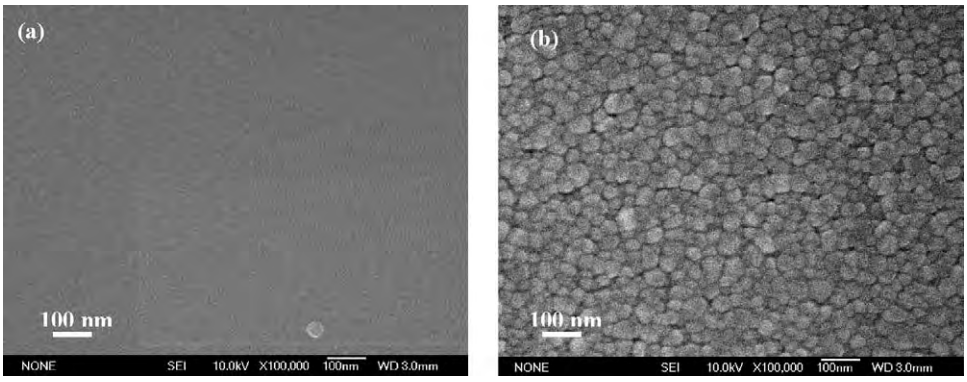

Fig. 33. SEM views of the ZrO_2 thin film: (a) as-deposited and (b) treated at 1000 °C for 2 h [145].

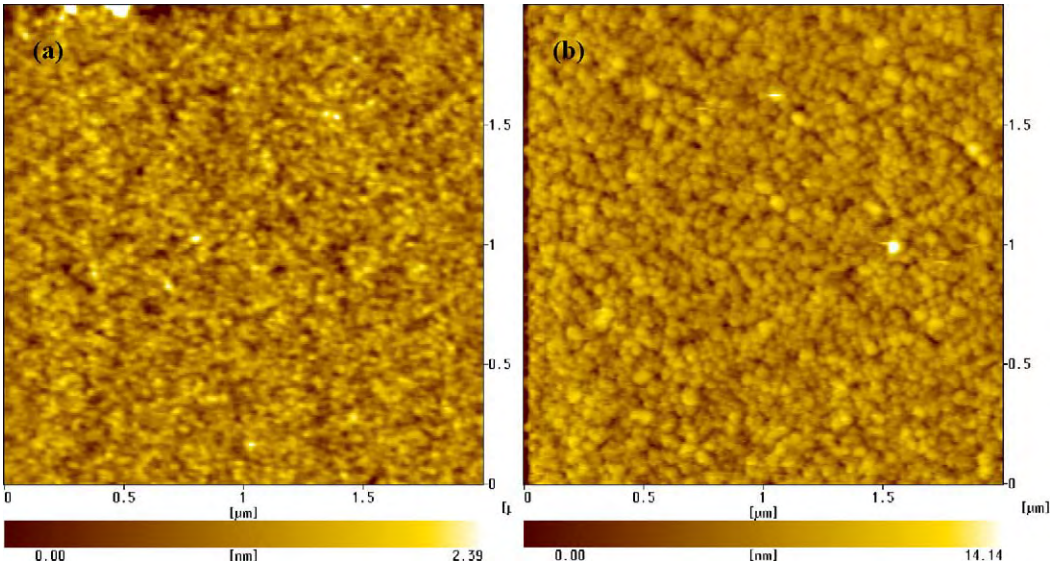

Fig. 34. AFM views of the ZrO_2 thin film: (a) as-depositedand and (b) treated at 1000 °C for 2 h [145].

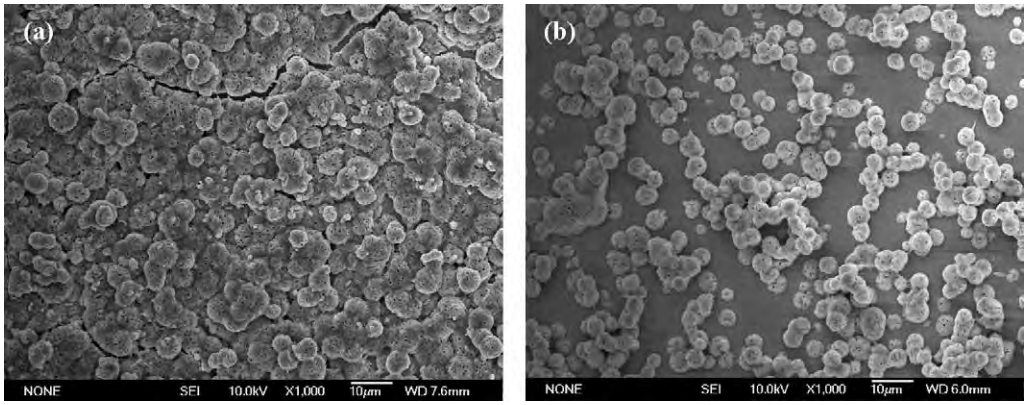

Fig. 35. Surface views of the different ZrO_2 thin film soaked in SBF for 28 days: (a) as-deposited and (b) thermal-treated at 1000 °C for 2 h [145].

surface grow to about 30–50 nm, as shown in Figs. 33b and 34b. The as-deposited and thermally treated ZrO_2 thin films are immersed in SBF to evaluate the bioactivity and the results are displayed in Fig. 35. After immersion in SBF for 28 days, the surface of the as-deposited ZrO_2 thin film is completely covered by the apatite layer, but relatively little apatite appears on the surface of the ZrO_2 thin film annealed at 1000 °C for 2 h. The results indicate that the bioactivity of the ZrO_2 thin film deteriorates due to thermal treatment and the size of the particles appears to be one of the key factors.

Ion plating is characterized by energetic bombardment of particles that alter the substrate surface and influence the film formation. The materials for deposition are vaporized by evaporation, sputtering, arc erosion, or decomposition of chemical precursors. The energetic particles are usually ions of an inert or reactive gas or in some cases, ions of the condensing film materials. Various ion plating processes such as arc ion plating and plasma immersion ion plating have been employed to prepare thin films. Ionic plasma deposition (IPD) is an efficient method to deposit nanostructured films onto a variety of materials including metals and polymers. Cohen et al. [146] have studied the osteoblast and fibroblast functions on silicone IPD-coated with titanium and claimed that the nanoroughness (features usually below100 nm) of the IPD-coated titanium enhances osteoblast functions while at the same time decreases fibroblast attachment and growth. The corrosion behavior of Ti6Al4V alloy with TiN and TiN/Ti films prepared by arc ion plating AIP has been evaluated in Hank's simulated body fluid and compared with that of the bare alloy. The deposited films show higher corrosion potential and polarization resistance as well as lower corrosion current density than the bare alloy, indicating that the two films can provide effective protection to Ti6Al4V [147]. A layer of tantalum with a roughness of 10.349 nm can be produced on TiNi alloy by the arc ion plating method [148]. The layer can inhibit release of Ni ions from the TiNi substrate. Yoshinari et al. [149] suggest that dry surface modification processes such as ion implantation, ion plating, ion beam mixing, and so on are useful in controlling the physico-chemical nature, such as the surface energy and surface electrical charge of surfaces, and development of tissue-compatible implants.

Ion implantation is also a PVD process in which ions are implanted into a solid. Ion implantation can be categorized into conventional beam-line ion implantation and plasma immersion ion implantation (PIII). PIII has shown potential due to its versatility in modifying the surface characteristics of biomaterials and implants with irregular shape such as surface structure, composition, functional groups, type of bonding bimolecular or cells, morphological feature of the surface, and so on [150]. The performance and long-term durability of medical implants are threatened by the presence of bacteria in the vicinity of the implant surfaces. In this respect, energetic silver and copper ions implanted into metallic [151] or nonmetallic [152,153] medical materials can render them with better antibacterial characteristics.

5.8. Chemical vapor deposition

In chemical vapor deposition, atoms or molecules produced by high temperature reduction or decomposition of chemical vapor precursors are deposited. The deposited materials may react with other gaseous species in the system to yield compounds. CVD covers a family of techniques such as vapor phase epitaxy (VPE) when CVD is used to deposit single crystal films, metalorganic CVD (MOCVD) when the precursor gases consist of metal-organic species, plasma enhanced CVD (PECVD) when plasmas are used to induce or enhance decomposition and reaction, and low pressure CVD (LPCVD) when the pressure is less than ambient.

Nanostructured silver coatings have been fabricated by flame assisted chemical vapor deposition [154]. As shown in Fig. 36, the film is produced via the Volmer-Weber growth mode which leads to isolated nanoparticles rather than a continuous film. Such nanostructured silver films have potential in enhanced biocidal to Gram negative bacteria E Coli. The silver nanoclusters can be embedded in an organosilicon matrix via a PECVD process [155]. It is believed that the antimicrobial property of the composite thin film is related to the Ag^+ ions that are progressively released from the embedded nanoparticles into the surrounding medium.

Nanocrystalline diamond (NCD) can be produced by microwave plasma enhanced CVD (MWPECVD) [156] or hot filament CVD [157]. On account of the superior hardness, low friction coefficient, high chemical resistance and feasibility to coat on a variety of

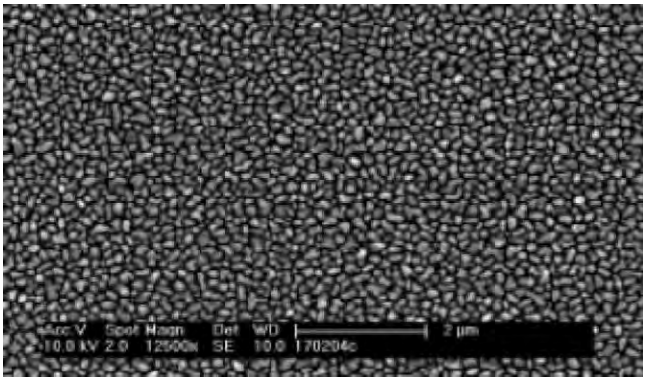

Fig. 36. SEM image showing silver islands grown on thick silica coated barrier glass substrates at a constant substrate temperature of 300 °C [154].

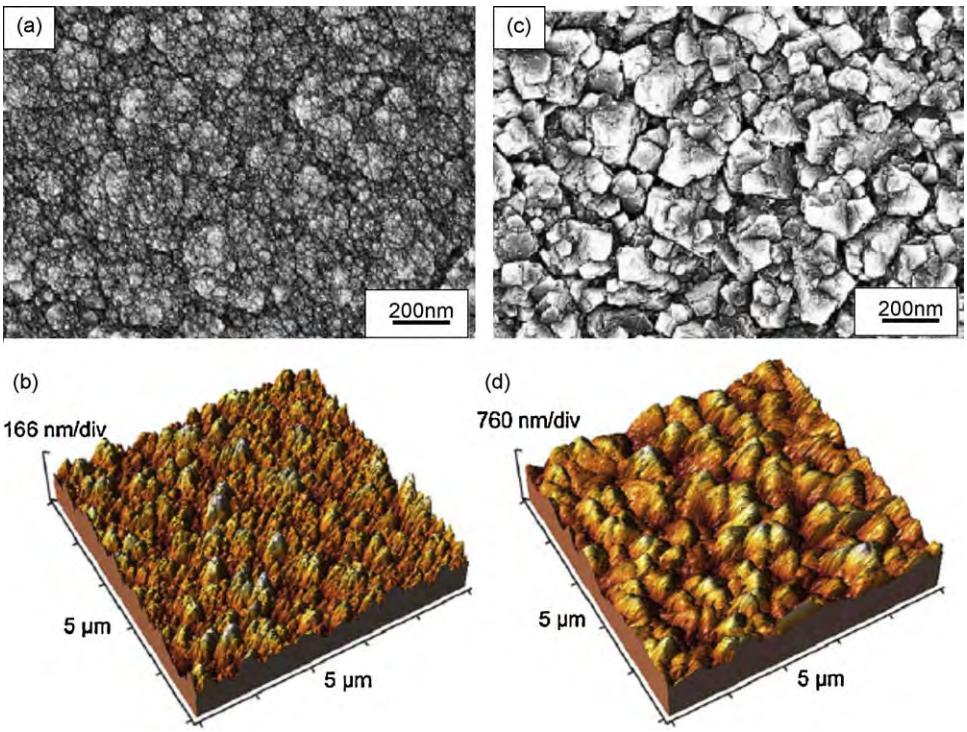

Fig. 37. (a and b) SEM and AFM images of NCD and (c and d) SMCD showing nano and submicron scale topographies, respectively [158].

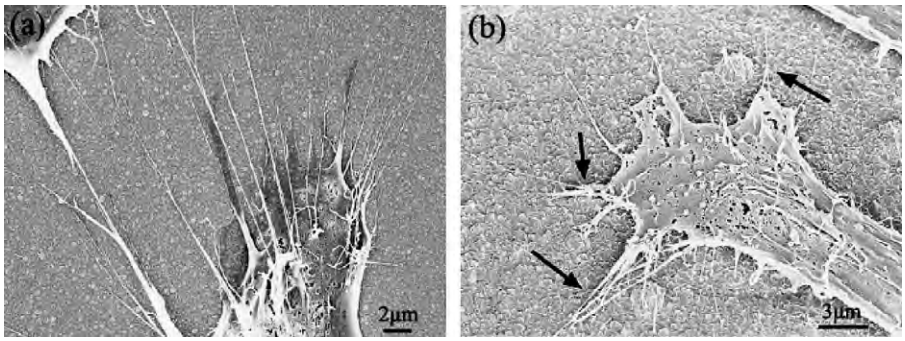

Fig. 38. (a) Osteoblast filopodia extensions on NCD and (b) SMCD after 48 h of culture. The arrows in (b) indicate filopodia extensions converging to some spots on the diamond surfaces. The osteoblast seeding density is 10,000 cells/cm^2 [158].

substrates, NCD has potential in biomedical applications, especially associated with enhanced orthopedic implant durability. Yang et al. [158] compare the functions of osteoblasts on nanocrystalline diamond and submicron crystalline diamond (SMCD) films fabricated by MWPECVD and hydrogen plasma treatment. The NCD and SMCD films show similar surface chemistry and wettability but different topographies as shown in Fig. 37. Osteoblast filopodia on the NCD show parallel extensions and the filopodia protrude radially from the membrane (Fig. 38). In contrast, on the SMCD, osteoblast filopodia are less protruded and tend to converge on specific spots, as shown in Fig. 38b (indicated by arrows). Osteoblast filopodia on the NCD are also longer than those on the SMCD. It is generally agreed that both short-term and long-term functions of osteoblasts are significantly enhanced on the NCD compared to SMCD.

Recently, other new nanotechniques such as polymer demixing [159], dip-pen lithography [160], photo- or electron-beam nanolithography [161,162], and imprint lithography [163] have been developed to construct a geometrically defined environment

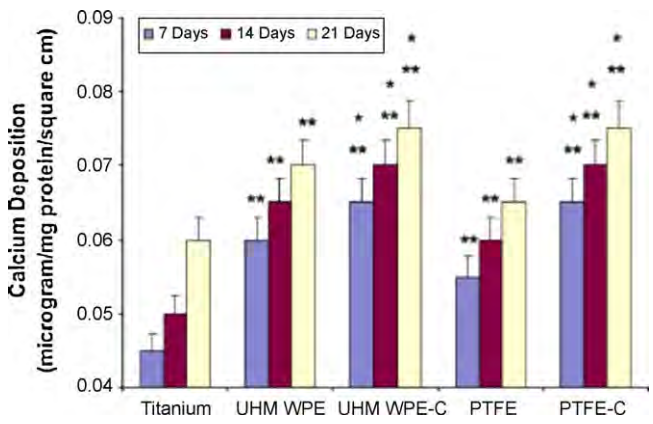

Fig. 39. Increased osteoblast calcium mineral deposition on UMMWPE and PTFE coated with nano Ti after 7, 14, and 21 days. Data = mean + SD, $n = 3$; $^{*}p < 0.01$ (compared to respective uncoated polymer sample) and $^{**}p < 0.01$ (compared to currently-used Ti, labeled as Titanium). C, coated with nano Ti using IPD [168].

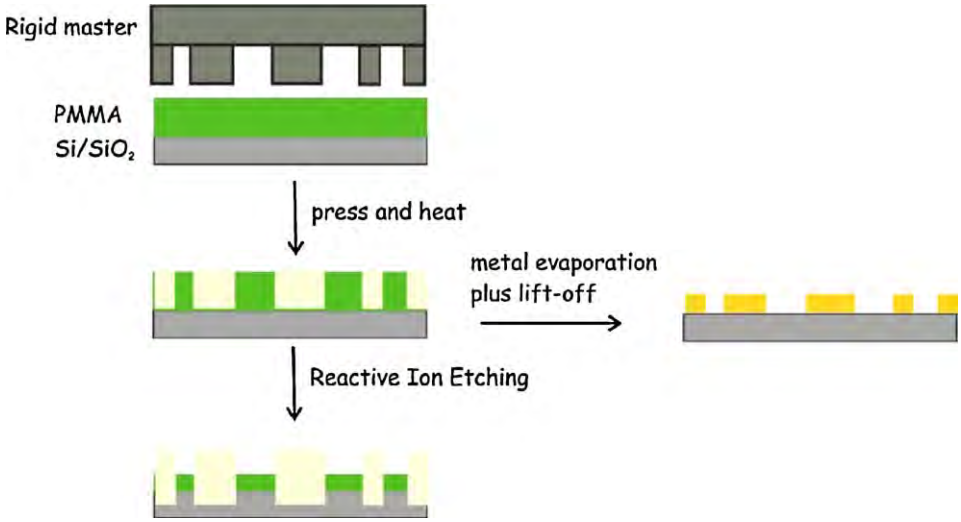

Fig. 40. Schematic overview of nanoimprint lithography. The rigid master is usually prepared via e-beam lithpgraphy and has feature sizes in the 10–100 nm size range. After imprinting the polymer film, further etching can transfer the pattern into the underlying substrate. Alternatively, metal evaporation and lift-off of the polymer mask produces nanopattern features [172].

for cells on the nanoscale. These fledgling techniques have led to more investigations of nanotopography-dependent mechanisms of integrin-mediated cell signaling [164].

6. Surface nano-functionalization of biopolymers

Nowadays, biopolymers are widely used in surgery, prosthetic systems, pharmacology, drug formulation, and controlled drug delivery. In order to obtain surface nano-functionalized biopolymers, surface modification techniques are used to deposit coatings/films, implant ions, and embed nanoparticles into the biopolymers.

6.1. Deposition of coatings/films

Osteoblasts are shown to selectively align on carbon nanofiber/nanotube arrays placed on several polymer matrices. The unique surface energetics of carbon nanofibers/nanotubes are capable of promoting adsorption of proteins and mediate subsequent bone cell adhesion [165]. Therefore, carbon nanotubes are intriguing biomaterials due to their unique biologically inspired surface, electrical, and mechanical properties. Khang et al. [166] first reported enhanced functions of chondrocytes (cartilage synthesizing cells) on electrically and nonelectrically stimulated highly dispersed carbon nanotubes in polycarbonate urethane (PCU) compared to stimulated pure PCU. The results confirm the combined role of nanosurface roughness and electrical stimulation on enhanced functions of chondrocytes and provide direct evidence on the positive role that conductive CNT/PCU films play in promoting functions of chondrocytes in cartilage regeneration. Kim et al. [167] have investigated macrophage functions on carbon nanotubes microscopically aligned on PCU. Their studies demonstrate decreased numbers of macrophages along aligned carbon

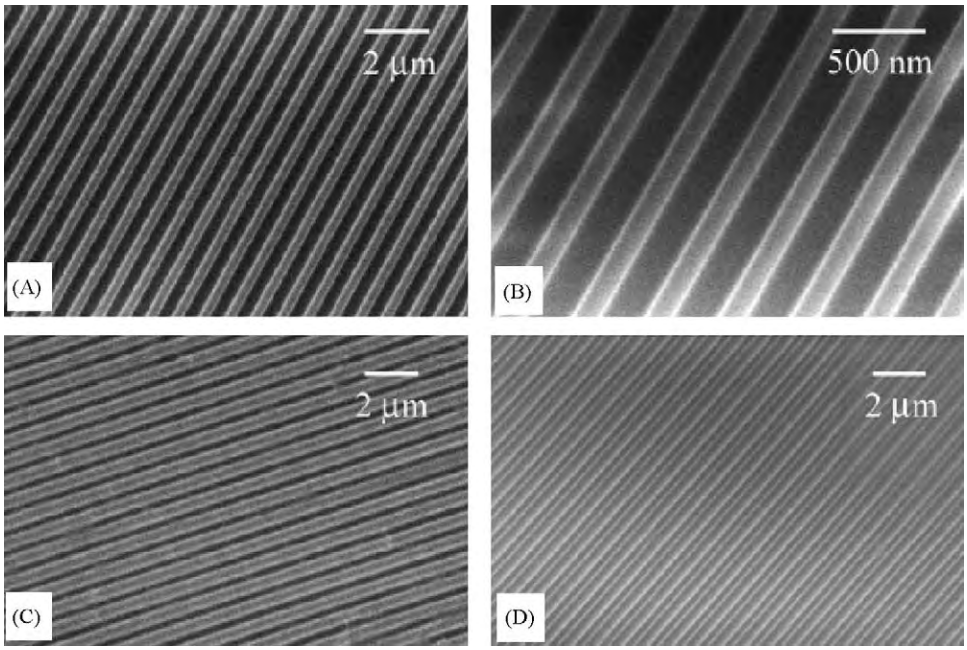

Fig. 41. Scanning electron micrographic of (A and B) nano-imprintred gratins on PMMA coating on SiO_2 wafer, (C) PDMS nanopatterned by replica molding, and (D) collagen coated PDMS with nanopatterns. Bar = 2 μm for A, C and D and bar = 500 nm for B [174].

nanotubes placed on polycarbonate urethane for 4 h, 24 h, and 4 days, indicating decreased macrophage activation on carbon nanotubes. Compared to PCU, decreasing macrophage functions are attributed to the increased nanometer surface roughness and unique surface energy of carbon nanotubes. Their result demonstrate that carbon nanotubes may suppress macrophage functions and decrease persistent wound healing responses that have undermined orthopedic implant efficacy to date.

Reising et al. [168] have also investigated the long-term functions of osteoblasts on several potential orthopedic polymeric materials such as ultrahigh molecular weight polyethylene (UHMWPE) and polytetrafluoroethylene (PTFE) coated with nanostructured titanium by ionic plasma deposition. The nanostructured surfaces are created on UHMWPE and PTEF by first using a vacuum to remove all contaminants and then guiding charged metallic ions or plasma to the surfaces at ambient temperature. The results demonstrate that compared to currently used titanium and uncoated polymers, polymers coated with titanium by IPD significantly increases osteoblast proliferation and calcium deposition, as shown in Fig. 39.

6.2. Chemical treatment

Chemical treatment methods are used to conduct surface nanofunctionalization of biopolymers. Park et al. [169] have reported that 2-dimensional NaOH-treated poly(lactic-co-glycolic acid) (PLGA)

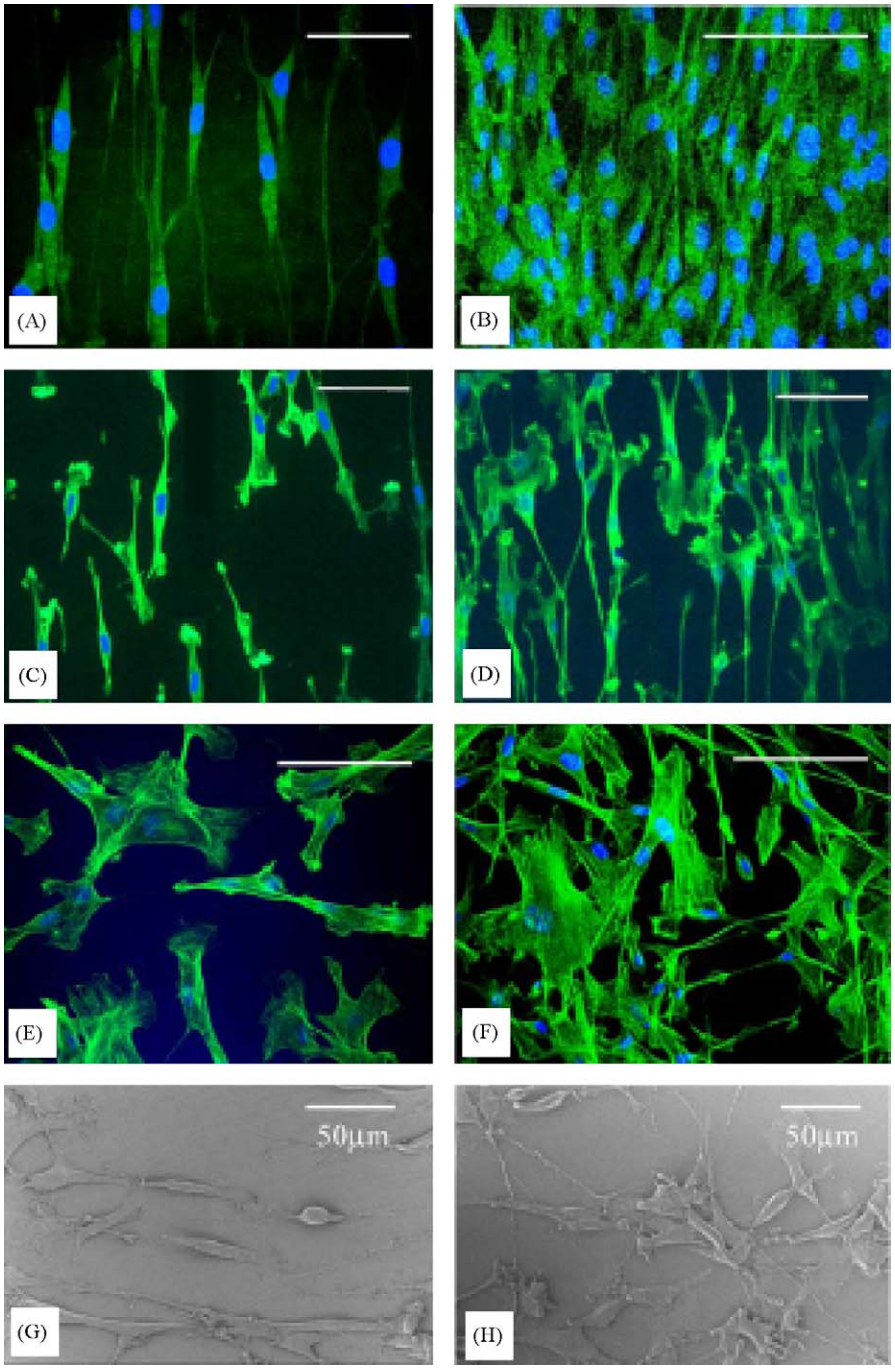

Fig. 42. Confocal micrographs of F-actin stained SMC on (A) nano-imprinted PMMA at low cell density, (B) nano-imprinted PMMA at high cell density, (C) nanopatterned PDMS at low cell density, (D) nano-patterned PDMS at high cell density, (E) non-patterned PMMA and (F) glass cover slip. Scanning electon micrographs of SMC cultured on (G) nano-imprinted gratings on PMMA coated on SiO_2 wafer and (H) non-patterned PMMA coated on SiO_2 wafer. Bar = 50 μm for all except (B) Bar = 100 μm [174].

substrates enhance functions of osteoblasts, vascular and bladder smooth muscle cells, and chondrocytes compared to conventional PLGA. Not only does the cell number increases on NaOH-treated PLGA scaffolds, but also subsequent functions of chondrocytes (such as collagen, GAG, and overall total protein synthesis) are enhanced. The microstructure and properties of PLGA can be varied by the NaOH treatment. For instance, a more hydrophilic surface, increased surface area, altered porosity, and a greater degree of nanometer roughness can be achieved and these are important factors affecting chondrocyte functions. Chung et al. [170] mix different molecular weights or chain lengths of polyethylene glycol (PEG) and then grafted them onto a polyurethane (PU) surface to model a smooth surface and to form nanometer (nm) scale roughness on PU-PEG surfaces (PU-PEGmix). Here, photochemical techniques are adopted to graft Gly–Arg–Gly–Asp (GRGD) peptide onto the PU-PEGmix surface by inducing photochemical reactions between the azido group and hydroxyl group of the PEG molecules. The work reveals that increased surface roughness of biomaterial surfaces even on the 10–100 nm scale can enhance the adhesion and growth of human endothelial cells (HUVECs).

6.3. Nanoimprint lithography

Nanoimprint lithography (NIL) is an emerging lithographic technology that promises high-throughput patterning of nanostructures. It was first proposed by Stephen Chou et al. of the University of Minnesota [171] and the schematic overview of NIL is displayed in Fig. 40 [172]. NIL can be used to pattern sub 10 nm features and yet it only requires simple equipment and easy processing. NIL involves three typical processes: hot embossing lithography (HEL), UV-based nanoimprint lithography (UV-NIL), and micro contact printing (μ-CP, MCP) [173]. NIL is considered one of the promising processes in next generation lithography due to its simplicity, low cost, high replication fidelity, and relatively high throughput. The quality of the nanoimprinting process depends on number of experimental parameters like T_g, viscosity in the melt, adhesion of the polymer to the mold, etc. PMMA has been most widely used as the imprintable materials, but various thermoplastic and thermosetting polymers are under investigation to optimize the imprinting and subsequent etching steps.

Yim et al. [174] have investigated the cell behavior such as morphology, proliferation, and motility of bovine pulmonary artery smooth muscle cells (SMC) on poly(methyl methacrylate) (PMMA) and poly(dimethylsiloxane) (PDMS) surfaces comprising nanopatterned gratings with 350 nm linewidth, 700 nm pitch, and 350 nm depth generated by nanoimprint lithography, as shown in Fig. 41. More than 90% of the cells align to the gratings and are significantly elongated compared to the SMC cultured on non-patterned surfaces, as shown in Fig. 42. The nuclei are also elongated and aligned. Cell proliferation is significantly reduced on the nanopatterned surfaces. Polarization of microtubule organizing centers (MTOC) associated with cell migration of SMC cultured on nanopatterned surfaces shows a preference towards the axis of cell alignment in the *in vitro* wound healing assay. In contrast, the MTOC of SMC on the non-patterned surface preferentially polarizes towards the wound edge. Curtis et al. [175] report that the ordered surface array of nanopits in polycaprolactone (PCL) and polymethylmethacrylate has marked effects on reducing adhesion compared to less regular arrays or planar surfaces. It is suggested that interfacial forces may be organized by the nanostructures to affect the cells in the same way liquid crystal orientations are altered.

6.4. Plasma polymerization

Plasma polymerization is a thin film deposition process to prepare polymeric films on a wide variety of substrates. Species excited in the plasma can undergo condensation reactions forming the polymeric materials. These reactions can occur either in the plasma or gas phase. The products can be varied from oily fluids to very hard, dense solids. The characteristics of plasma polymers can be controlled by the power, pressure, and flow rate of the monomer gas. Carrier gases such as Ar, O_2, or H_2 also have an effect on the properties of some plasma polymers. Compared to conventional polymers, plasma polymers have some unique advantages including ultra-thin film deposition, and good adhesion, and they have a stable, durable nature with similar the same bulk properties. Therefore, plasma deposition has become an important technique to develop biomaterials with specific surface properties such as hydrophilicity [176], blood compatibility [177,178] and controlled drug release [179,180].

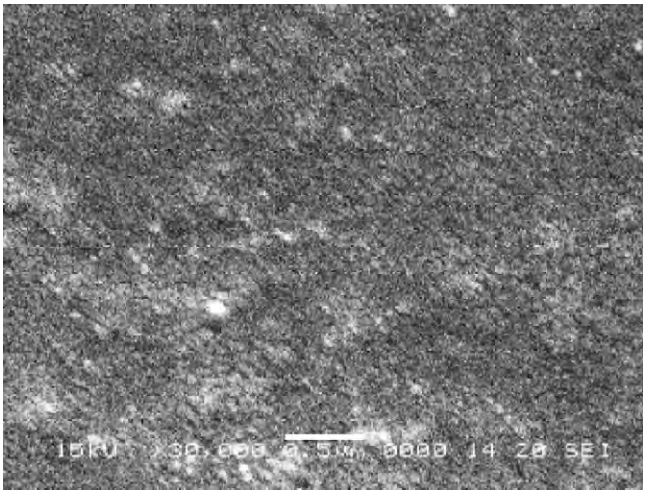

Fig. 43. SEM micrographs of PPBMA coating in case of deposition without oxygen [181].

Yuan et al. [181] have investigated the effects of oxygen gas on the chemical structure, surface morphology, hydrophilicity, and drug-controlled release characteristics of RF plasma poly-n-butyl methacrylate (PPBMA) films. The drug eluting system used in the release experiments consists of polyethylene vinylacetate (EVA)/paclitaxel matrix on 316L stainless steel. Oxygen has little influence on the chemical structure of PPBMAs. The dome-like structure with nano-sized particles is produced during deposition without oxygen (Fig. 43) and a smooth and dense surface is produced with oxygen. After deposition with oxygen, the hydrophilicity of PPBMA is higher than that without oxygen. Drug

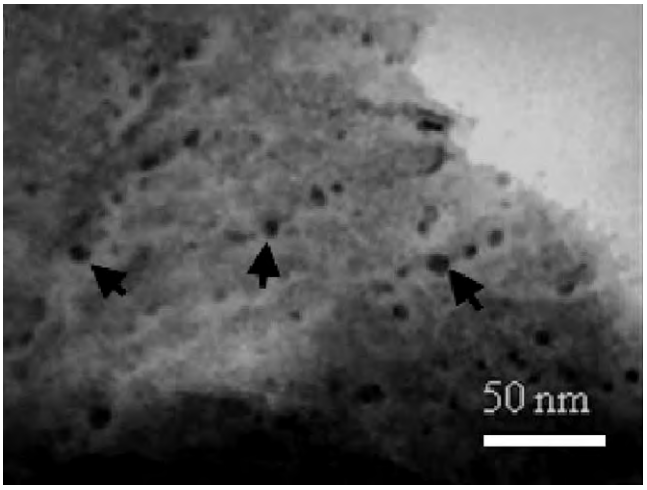

Fig. 44. Cross-sectional TEM image of Ag PIII polyethylene [182].

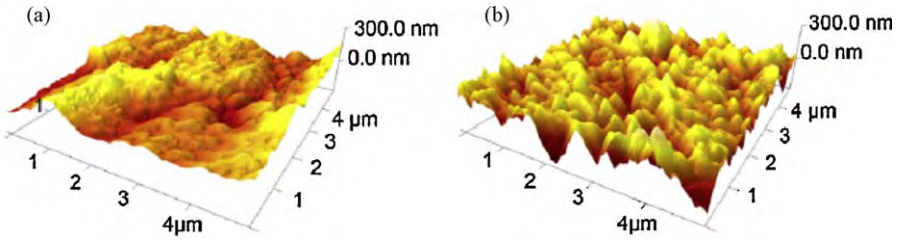

Fig. 45. 3D AFM images of (a) untreated PTFE substrate and (b) long pulse, high frequency treated PTFE [183].

release from the PPBMA coating deposited without oxygen shows the biphasic patterns, but the one with oxygen exhibits a slow Higuchi release.

6.5. Plasma immersion ion implantation

Plasma immersion ion implantation is a viable technique to implant antibacterial metals into polymers to enhance the antibacterial properties. Zhang et al. [182] have studied the antibacterial properties of Ag and Ag/N_2 implanted polyethylene surfaces and revealed that the implanted Ag ions tend to segregate into nano silver particles in the polymer matrix (as shown by the black arrows in Fig. 44) rather than distribute in the atomic state. Antibacterial tests disclose that Ag/N_2 co-PIII can prolong the antibacterial effects of the modified surfaces. On the other hand, the surface morphology (roughness) of the substrate is modified by PIII because of energetic ion bombardment. Wang et al. [183] have studied the effects of the pulse width and frequency on the surface roughness of polytetrafluoroethylene in oxygen PIII. It is demonstrated that after long pulse, high frequency (pulse duration of 200 ms and frequency of 500 Hz) O_2 PIII, the PTFE surface becomes superhydrophobic due to the formation of less oxygen groups and rougher surface morphology as shown by the sharp rods with sizes of about hundreds of nanometers in Fig. 45. However, only long pulse, high frequency O_2 PIII up-regulates the OCN expression of the seeded osteoblasts compared to the untreated PTFE and this effect is not obvious after short pulse/low frequency O_2 PIII and O_2 plasma treated PTFE. Consequently, long pulse, high frequency O_2 PIII process is more promising from the perspective of surface modification of PTFE to be used as bone or cartilage replacements.

7. Conclusion

The surface of biomaterials such as ceramics, metals, and polymers can be nano-functionalized by various surface modification techniques. The nano-functionalized surfaces are shown to affect cellular and subcellular functions significantly and have promising biological properties. Consequently, research pertaining to surface nano-functionalization of biomaterials has attracted much attention and a wealth of knowledge has been accumulated. However, better and simpler techniques need to be developed in order to control the surface nanostructures more precisely. Moreover, it is important to evaluate the safety of the nano-functionalized surfaces before clinical uses.

Acknowledgements

This work was jointly supported by Shanghai Science and Technology R&D Fund under grant 0952nm04400, 07JC14057, 0852nm03300 and 08ZR1421600, National Basic Research Fund under grant 2005CB623901, National Natural Science Foundation of China 30700170, Shanghai-Unilever Research and Development Fund 09520715200, City University of Hong Kong Strategic Research Grant (SRG) No. 7008009, and Hong Kong Research Grants Council (RGC) General Research Funds (GRF) No. CityU 112307.

References

[1] G. Balasundaram, T.J. Webster, J. Mater. Chem. 16 (2006) 3737–3745.
[2] S.C.G. Leeuwenburgh, J.A. Jansen, J. Malda, A.D. Wouter, J. Rouwkema, C.A. Van Blitterswijk, C.J. Kirkpatrick, D.F. Williams, Biomaterials 29 (2008) 3047–3052.
[3] M.M. Stevens, J.H. George, Science 310 (2005) 1135–1138.
[4] C.J. Wilson, R.E. Clegg, D.I. Leavesley, M.J. Pearcy, Tissue Eng. 11 (2005) 1–18.
[5] T.J. Webster, J.U. Ejiofor, Biomaterials 25 (2004) 4731–4739.
[6] R.L. Price, M.C. Waid, K.M. Haberstroh, T.J. Webster, Biomaterials 24 (2003) 1877–1887.
[7] T.J. Webster, T.A. Smith, J. Biomed. Mater. Res. 74A (2005) 677–686.
[8] I. Manjubala, S. Scheler, J. Bossert, K.D. Jandt, Acta Biomater. 2 (2006) 75–84.
[9] T.A. Desai, Med. Eng. Phys. 22 (2001) 595–606.
[10] J. Aizenberg, Bell Labs Tech. J. 10 (2005) 129–141.
[11] L. Feng, S.H. Li, Y.S. Li, H.J. Li, L.J. Zhang, J. Zhai, Y.L. Song, B.Q. Liu, L. Jiang, D.B. Zhu, Adv. Mater. 14 (2002) 1857–1860.
[12] X.J. Feng, L. Jiang, Adv. Mater. 18 (2006) 3063–3078.
[13] T. Wagner, C. Neinhuis, W. Barthlott, Acta Zool. 77 (1996) 213–225.
[14] W. Lee, M.K. Jin, W.C. Yoo, J.K. Lee, Langmuir 20 (2004) 7665–7669.
[15] P. Fratzl, H.S. Gupta, E.P. Paschalis, P. Roschger, J. Mater. Chem. 14 (2004) 2115–2123.
[16] X.Y. Liu, P.K. Chu, C.X. Ding, Mater. Sci. Eng. R 47 (2004) 49–121.
[17] T.J. Webster, R.W. Siegel, R. Bizios, Biomaterials 20 (1999) 1221–1227.
[18] T.J. Webster, C. Ergun, R.H. Doremus, R.W. Siegel, R. Bizios, Biomaterials 21 (2000) 1803–1810.
[19] T.J. Webster, C. Ergun, R.H. Doremus, R.W. Siegel, R. Bizios, Biomaterials 22 (2001) 1327–1333.
[20] K.L. Elias, R.L. Price, T.J. Webster, Biomaterials 23 (2002) 3279–3287.
[21] T.J. Webster, E.L. Hellenmeye, R.L. Price, Biomaterials 26 (2005) 953–960.
[22] L.G. Gutwein, T.J. Webster, Biomaterials 25 (2004) 4175–4183.
[23] G. Balasundaram, M. Sato, T.J. Webstera, Biomaterials 27 (2006) 2798–2805.
[24] C. Ergun, H. Liu, T.J. Webster, E. Olcay, S. Yılmaz, F.C. Sahin, J. Biomed. Mater. Res. 85A (2008) 236–241.
[25] N. Sinha, J.T.W. Yeow, IEEE T. Nanobiosci. 4 (2005) 180–195.
[26] R.A. MacDonald, B.F. Laurenzi, G. Viswanathan, P.M. Ajayan, J.P. Stegeman, J. Biomed. Mater. Res. 74A (2005) 489–496.
[27] A.R. Boccaccini, F. Chicatun, J. Cho, O. Bretcanu, J.A. Roether, S. Novak, Q.Z. Chen, Adv. Funct. Mater. 17 (2007) 2815–2822.
[28] B.C. Ward, T.J. Webster, Mater. Sci. Eng. C 27 (2007) 575–578.
[29] E. McCafferty, J.P. Wightman, Appl. Surf. Sci. 143 (1999) 92–100.
[30] F. Variola, J.H. Yi, L. Richert, J.D. Wuest, F. Rosei, A. Nanci, Biomaterials 29 (2008) 1285–1298.
[31] H.M. Kim, F. Miyaji, T. Kokubo, T. Nakamura, J. Biomed. Mater. Res. 32 (1996) 409–417.
[32] J.M. Wu, J. Cryst. Growth 269 (2004) 347–355.
[33] J.M. Wu, T.W. Zhang, Langmuir 21 (2005) 6995–7002.
[34] J.M. Wu, B. Huang, M. Wang, A. Osaka, J. Am. Ceram. Soc. 89 (2006) 2660–2663.
[35] J.M. Wu, H.X. Xue, J. Am. Ceram. Soc. 92 (2009) 2139–2143.
[36] Y.H. Wu, M.C. Long, W.M. Cai, S.D. Dai, C. Chen, D.Y. Wu, J. Bai, Nanotechnology 20 (2009) 185703.
[37] E. Hosono, H. Matsuda, I. Honma, M. Ichihara, H.S. Zhou, Langmuir 23 (2007) 7447–7450.
[38] G.S. Shi, L.F. Ren, L.Z. Wang, H.S. Lin, S.B. Wang, Y.Q. Tong, Oral Surg. Oral Med. Oral Pathol. Oral Radiol. Endod. 108 (2009) 368–375.
[39] X.X. Wang, S. Hayakawa, K. Tsuru, A. Osaka, Biomaterials 23 (2002) 1353–1357.
[40] M.H. Lee, I.S. Park, K.S. Min, S.G. Ahn, J.M. Park, K.Y. Song, C.W. Park, Met. Mater. Int. 2 (2007) 109–115.
[41] M. Sun, Wang, Appl. Surf. Sci. 255 (2008) 396–400.
[42] J.L. Guo, R.J. Padilla, W. Ambrose, I.J.D. Kok, L.F. Cooper, Biomaterials 28 (2007) 5418–5425.
[43] S.F. Lamolle, M. Monjo, M. Rubert, H.J. Haugen, S.P. Lyngstadaas, J.E. Ellingsen, Biomaterials 30 (2009) 736–742.
[44] M. Uchida, A. Oyane, H.M. Kim, T. Kokubo, A. Ito, Adv. Mater. 16 (2004) 1071–1074.
[45] S.L. Wu, X.M. Liu, T. Hu, P.K. Chu, J.P.Y. Ho, Y.L. Chan, K.W.K. Yeung, C.L. Chu, T.F. Hung, K.F. Huo, C.Y. Chung, W.W. Lu, K.M.C. Cheung, K.D.K. Luk, Nano Lett. 8 (2008) 3803–3808.
[46] T. Miyazaki, H.M. Kim, F. Miyaji, T. Kokubo, H. Kato, T. Nakamura, J. Biomed. Mater. Res. 50 (2000) 35–42.
[47] M. Uchida, H.M. Kim, F. Miyaji, T. Kokubo, T. Nakamura, Biomaterials 23 (2002) 313–317.

[48] H. Masuda, K. Fukuda, Science 268 (1995) 1466–1468.
[49] V. Zwilling, C.E. Darque, F.A. Boutry, D. David, M.Y. Perrin, M. Aucouturier, Surf. Interface Anal. 27 (1999) 629–637.
[50] D.W. Gong, C.A. Grimes, O.K. Varghese, W.C. Hu, R.S. Singh, Z. Chen, E.C. Dickey, J. Mater. Res. 16 (2001) 3331–3334.
[51] C.A. Grimes, J. Mater. Chem. 17 (2007) 1451–1457.
[52] G.A. Crawford, N. Chawla, Acta Mater. 57 (2009) 854–867.
[53] J.M. Macak, H. Tsuchiya, P. Schmuki, Angew. Chem. Int. Ed. 44 (2005) 2100–2102.
[54] J.M. Macak, H. Tsuchiya, L. Taveira, S. Aldabergerova, P. Schmuki, Angew. Chem. Int. Ed. 44 (2005) 7463–7465.
[55] M. Paulose, K. Shankar, S. Yoriya, H.E. Prakasam, O.K. Varghese, G.K. Mor, T.A. Latempa, A. Fitzgerald, C.A. Grimes, J. Phys. Chem. B 110 (2006) 16179–16184.
[56] S.P. Albu, A. Ghicov, S. Aldabergenova, P. Drechsel, D. LeClere, G.E. Thompson, J.M. Macak, P. Schmuki, Adv. Mater. 20 (2008) 4135–4139.
[57] S.P. Albu, D. Kim, P. Schmuki, Angew. Chem. Int. Ed. 47 (2008) 1916–1919.
[58] D.A. Wang, Y. Liu, B. Yu, F. Zhou, W.M. Liu, Chem. Mater. 21 (2009) 1198–1206.
[59] A. Ghicov, P. Schmuki, Chem. Commun. 20 (2009) 2791–2808.
[60] H. Tsuchiya, J.M. Macak, L. Müller, J. Kunze, F. Müller, P. Greil, S. Virtanen, P. Schmuki, J. Biomed. Mater. Res. 77A (2006) 534–541.
[61] J. Kunze, L. Muller, J.M. Macak, P. Greil, P. Schmuki, F.A. Muller, Electrochim. Acta 53 (2008) 6995–7003.
[62] J. Park, S. Bauer, K. Van der Mark, P. Schmuki, Nano Lett. 7 (2007) 1686–1691.
[63] J. Park, S. Bauer, K.A. Schlegel, F.W. Neukam, K. Von der Mark, P. Schmuki, Small 5 (2009) 666–671.
[64] S. Oh, C. Daraio, L.H. Chen, T.R. Pisanic, R.R. Fin"ones, S. Jin, J. Biomed. Mater. Res. 78A (2006) 97–103.
[65] A. Aumelas, A. Serrero, A. Durand, E. Dellacherie, M. Leonard, Colloids Surf. B 59 (2007) 74–80.
[66] Y.Y. Song, F. Schmidt-Stein, S. Bauer, P. Schmuki, J. Am. Chem. Soc. 131 (2009) 4230–4232.
[67] C. Yao, T.J. Webster, J. Biomed. Mater. Res. 91B (2009) 587–595.
[68] A.L. Yerokhin, X. Nie, A. Leyland, A. Matthews, S.J. Dowey, Surf. Coat. Tech. 122 (1999) 73–93.
[69] Y. Han, S.H. Hong, K.W. Xu, Surf. Coat. Tech. 154 (2002) 314–318.
[70] Y. Han, D.H. Chen, J.F. Sun, Y.M. Zhang, K.W. Xu, Acta Biomater. 4 (2008) 1518–1529.
[71] Y.Y. Yan, Y. Han, Surf. Coat. Tech. 201 (2007) 5692–5695.
[72] Y.M. Wang, B.L. Jiang, T.Q. Lei, L.X. Guo, Surf. Coat. Tech. 201 (2006) 82–89.
[73] R. Arrabal, E. Matykina, F. Viejo, P. Skeldon, G.E. Thompson, Corros. Sci. 50 (2008) 1744–1752.
[74] F.Y. Jin, P.K. Chu, K. Wang, J. Zhao, A.P. Huang, H.H. Tong, Mater. Sci. Eng. A 476 (2008) 78–82.
[75] Y.K. Shin, W.S. Chae, Y.W. Song, Y.M. Sung, Electrochem. Commun. 8 (2006) 465–470.
[76] L. Ceschini, E. Lanzoni, C. Martini, D. Prandstraller, G. Sambogna, Wear 264 (2008) 86–95.
[77] Y.K. Jun, H.S. Kim, J.H. Lee, S.H. Hong, Sens. Actuators B 120 (2006) 69–73.
[78] H. Ishizawa, M. Ogino, J. Biomed. Mater. Res. 29 (1995) 65–72.
[79] W.H. Song, Y.K. Jun, Y. Han, S.H. Hong, Biomaterials 25 (2004) 3341–3349.
[80] B.H. Zhao, I.S. Lee, I.H. Han, J.C. Park, S.M. Chung, Curr. Appl. Phys. 7S1 (2007) e6–e10.
[81] Y.T. Sul, Biomaterials 24 (2003) 3893–3907.
[82] L.H. Li, Y.M. Kong, H.W. Kim, Y.W. Kim, H.E. Kim, S.J. Heo, J.Y. Koak, Biomaterials 25 (2004) 2867–2875.
[83] Y. Li, I.S. Lee, F.Z. Cui, S.H. Choi, Biomaterials 29 (2008) 2025–2032.
[84] D.Q. Wei, Y. Zhou, D.C. Jia, Y.M. Wang, Acta Biomater. 3 (2007) 817–827.
[85] M.S. Kim, J.J. Ryu, Y.M. Sung, Electrochem. Commun. 9 (2007) 1886–1891.
[86] Z.P. Yao, H.H. Gao, Z.H. Jiang, F.P. Wang, J. Am. Ceram. Soc. 91 (2008) 555–558.
[87] Y. Han, D.H. Chen, L. Zhang, Nanotechnology 19 (2008) 335705.
[88] A. Bai, Z.J. Chen, Surf. Coat. Tech. 203 (2009) 1956–1963.
[89] Y.Y. Yan, Y. Han, C.G. Lu, Appl. Surf. Sci. 254 (2008) 4833–4839.
[90] L.D. Piveteau, in: D.M. Brunette, P. Tengvall, M. Textor, P. Thomsen (Eds.), Titanium in Medicine, Springer, Berlin, 2001, pp. 267–282.
[91] C.J. Brinker, A.J. Hurd, P.R. Schunk, G.C. Frye, C.S. Ashley, J. Non-Cryst. Solids 147 (1992) 424–436.
[92] S. Sakka, in: M.A. Aegerter, M.J. Jafelicci, D.F. Souza, E.D. Zanotto (Eds.), Sol-gel Science and Technology: Sol-gel Fibers and Coating Films, World Scientific, Brazil, 1989, pp. 346–374.
[93] M.C. Advincula, F.G. Rahemtulla, R.C. Advincula, E.T. Ada, J.E. Lemons, S.L. Bellis, Biomaterials 27 (2006) 2201–2212.
[94] G. He, J. Hu, S.C. Wei, J.H. Li, X.H. Liang, E. Luo, Appl. Sur. Sci. 255 (2008) 442–445.
[95] T. Peltola, M. Pätsi, H. Rahiala, I. Kangasniemi, A. Yli-urpo, J. Biomed. Mater. Res. 41 (1998) 504–510.
[96] M. Jokinen, M. Pätsi, H. Rahiala, T. Peltola, M. Ritala, J.B. Rosenholm, J. Biomed. Mater. Res. 42 (1998) 295–302.
[97] S.K. Dinesh, M.S. Shashikanth, M.L. Yuri, K.M. David, Biomaterials 27 (2006) 4296–4303.
[98] J.X. Liu, D.Z. Yang, F. Shi, Y.J. Cai, Thin Solid Films 429 (2003) 225–230.
[99] E. Eisenbarth, D. Velten, J. Breme, Biomol. Eng. 24 (2007) 27–32.
[100] Y. Zeng, S.W. Lee, L. Gao, C. Ding, J. Eur. Ceram. Soc. 22 (2002) 347–351.
[101] B. Liang, C. Ding, H. Liao, C. Coddet, Surf. Coat. Tech. 200 (2006) 4549–5455.
[102] B. Liang, C. Ding, Surf. Coat. Tech. 191 (2005) 267–273.
[103] B. Liang, C. Ding, H. Liao, C. Coddet, J. Eur. Ceram. Soc. 29 (2009) 2267–2273.
[104] G.C. Wang, X.Y. Liu, J.H. Gao, C.X. Ding, Acta Biomater. 5 (2009) 2270–2278.
[105] X.Y. Liu, X.B. Zhao, R.K.Y. Fu, J.P.Y. Ho, C.X. Ding, P.K. Chu, Biomaterials 26 (2005) 6143–6150.
[106] X.Y. Liu, X.B. Zhao, C.X. Ding, P.K. Chu, Appl. Phys. Lett. 88 (2006) 013905.
[107] X.Y. Liu, X.B. Zhao, B. Li, C. Cao, Y.Q. Dong, C.X. Ding, P.K. Chu, Acta Biomater. 4 (2008) 544–552.
[108] M. Svetina, L.C. Ciacchi, O. Sbaizero, S. Meriani, A. de Vita, Acta Mater. 49 (2001) 2169–2177.
[109] P.J. Li, C. Ohtsuki, T. Kokubo, K. Nakanishi, N. Soga, K. de Groot, J. Biomed. Mater. Res. 28 (1994) 7–15.
[110] L. Vayssières, C. Chanéac, E. Trone, J.P. Joliver, J. Colloid. Interface Sci. 205 (1998) 205–212.
[111] H. Zhang, R.L. Penn, R.J. Hamers, J.F. Banfield, J. Phys. Chem. B 103 (1999) 4656–4662.
[112] W.P. Tong, N.R. Tao, Z.B. Wang, J. Lu, K. Lu, Science 299 (2003) 686–688.
[113] X. Wu, N. Tao, Y. Hong, B. Xu, J. Lu, K. Lu, Acta Mater. 50 (2002) 2075–2084.
[114] N.R. Tao, Z.B. Wang, W.P. Tong, M.L. Sui, J. Lu, K. Lu, Acta Mater. 50 (2002) 4603–4616.
[115] N.R. Tao, M.L. Sui, J. Lu, K. Lu, Nanostruct. Mater. 11 (1999) 433–440.
[116] H.W. Zhang, Z.K. Hei, G. Liu, J. Lu, K. Lu, Acta Mater. 51 (2003) 1871–1881.
[117] G. Liu, J. Lu, K. Lu, Mater. Sci. Eng. A 286 (2000) 91–95.
[118] D.H. Shin, I. Kim, J. Kim, Y.S. Kim, S.L. Semiatin, Acta Mater. 51 (2003) 983–996.
[119] A.V. Sergueeva, V.V. Stolyarov, R.Z. Valiev, A.K. Mukherjee, Scripta Mater. 45 (2001) 747–752.
[120] K.Y. Zhu, A. Vassel, F. Brisset, K. Lu, J. Lu, Acta Mater. 52 (2004) 4101–4110.
[121] F.A. Guo, K.Y. Zhu, N. Trannoy, J. Lu, Thermochim. Acta 419 (2004) 239–246.
[122] M. Wen, J.F. Gu, G. Liu, Z.B. Wang, J. Lu, Appl. Surf. Sci. 254 (2008) 2905–2910.
[123] M. Wen, J.F. Gu, G. Liu, Z.B. Wang, J. Lu, Surf. Coat. Tech. 201 (2007) 6285–6289.
[124] M. Wen, G. Liu, J.F. Gu, W.M. Guan, J. Lu, Surf. Coat. Tech. 202 (2008) 4728–4733.
[125] L. Zhang, Y. Han, J. Lu, Nanotechnology 19 (2008) 165706.
[126] D.M. Mattox, Handbook of Physical Vapor Deposition (PVD) Processing: Film Formation, Adhesion. Surface Preparation and Contamination Control, Noyes Publications, New Jersey, 1998.
[127] N.A. Shah, J. Coat. Technol. Res., DOI:10.1007/s11998-009r-r9211-3.
[128] M.V. Gorokhov, V.M. Kozhevin, D.A. Yavsin, S.A. Gurevich, Tech. Phys. 53 (2008) 1146–1151.
[129] Y. Yamada, K. Kouno, H. Kato, Y. Kobayashi, Hyperfine Interact. 182 (2008) 65–75.
[130] T. Kocourek, M. Jelinek, V. Vorlíček, J. Zemek, T. Jaňca, V. Žížková, J. Podlaha, C. Popov, Appl. Phys. A 93 (2008) 627–632.
[131] T.M. Patz, A. Doraiswamy, R.J. Narayan, N. Menegazzo, C. Kranz, B. Mizaikoff, Y. Zhong, R. Bellamkonda, J.D. Bumgardner, S.H. Elder, X.F. Walboomers, R. Modi, D.B. Chrisey, Mater. Sci. Eng. C 27 (2007) 514–522.
[132] L. Harris, A. Doraiswamy, R.J. Narayan, T.M. Patz, D.B. Chrisey, Mater. Sci. Eng. C 28 (2008) 359–365.
[133] T.M. Byrne, L. Lohstreter, M.J. Filiaggi, Z.J. Bai, J.R. Dahn, Surf. Sci. 603 (2009) 992–1001.
[134] C. Liu, Q. Zhao, Y. Liu, S. Wang, E.W. Abel, Colloid Surf. B 61 (2008) 182–187.
[135] L. Zhang, P. Lv, Z.Y. Huang, S.P. Lin, D.H. Chen, S.R. Pan, M. Chen, Diam. Relat. Mater. 17 (2008) 1922–1926.
[136] V. Karagkiozaki, S. Logothetidis, N. Kalfagiannis, S. Lousinian, G. Giannoglou, Nanomedicine: NBE 5 (2009) 64–72.
[137] H.C. Cheng, S.Y. Chiou, C.M. Liu, M.H. Lin, C.C. Chen, K.L. Ou, J. Alloys Compd. 477 (2009) 931–935.
[138] T. Xu, L. Pruitt, J. Mater. Sci.-Mater. M 10 (1999) 83–90.
[139] S.C.H. Kwok, W. Zhang, G.J. Wan, D.R. McKenzie, M.M.M. Bilek, P.K. Chu, Diam. Relat. Mater. 16 (2007) 1353–1360.
[140] N.W. Khun, E. Liu, X.T. Zeng, Corros. Sci. 51 (2009) 2158–2164.
[141] Y.T. Xie, X.B. Zheng, C.X. Ding, X.Y. Liu, P.K. Chu, Mater. Chem. Phys. 109 (2008) 342–346.
[142] Y.X. Leng, J.Y. Chen, H. Sun, P. Yang, G.J. Wan, J. Wang, N. Huang, Surf. Coat. Tech. 176 (2004) 141–147.
[143] Y.X. Leng, J.Y. Chen, J. Wang, G.J. Wan, H. Sun, P. Yang, N. Huang, Surf. Coat. Tech. 201 (2006) 157–163.
[144] X.Y. Liu, A.P. Huang, C.X. Ding, P.K. Chu, Biomaterials 27 (2006) 3904–3911.
[145] X.Y. Liu, P.K. Chu, C.X. Ding, in: D. ILA, J. Baglin, N. Kishimoto, P.K. Chu (Eds.), Ion-Beam-Based-Nanofabrication, Materials Research Society Symposium Proceeding, vol. 1020, 2007, pp. 81–89.
[146] A. Cohen, P. Liu-Synder, D. Storey, T.J. Webster, Nanoscale Res. Lett. 2 (2007) 385–390.
[147] B. Tian, D.B. Xie, F.H. Wang, J. Appl. Electrochem. 39 (2009) 447–453.
[148] Y. Cheng, W. Cai, Y.F. Zheng, H.T. Li, L.C. Zhao, Surf. Coat. Tech. 190 (2005) 428–433.
[149] M. Yoshinari, Y. Oda, T. Inoue, M. Shimono, Metall. Mater. Trans. A 33 (2002) 511–519.
[150] N. Huang, P. Yang, Y.X. Leng, J. Wang, H. Sun, J.Y. Chen, G.J. Wan, Surf. Coat. Tech. 186 (2004) 218–226.
[151] Y.Z. Wan, S. Raman, F. He, Y. Huang, Vacuum 81 (2007) 1114–1118.
[152] J. Wang, J.X. Li, L.R. Shen, L.A. Ren, Z.J. Xu, A.S. Zhao, Y.X. Leng, N. Huang, Nucl. Instrum. Meth. B 257 (2007) 141–145.
[153] W. Zhang, Y.J. Luo, H.Y. Wang, S.H. Pu, P.K. Chu, Surf. Coat. Tech. 203 (2009) 2550–2553.
[154] W.S. David, A.B. Lucy, M.Y. Heather, Chem. Vapor Depos. 14 (2008) 14–24.
[155] C. Saulou, B. Despax, P. Raynaud, S. Zanna, P. Marcus, M. Mercier-Bonin, Appl. Surf. Sci. 256S (2009) S35–S39.
[156] O.A. Williams, M. Nesladek, M. Daenen, S. Michaelson, A. Hoffman, E. Osawa, K. Haenen, R.B. Jackman, Diam. Relat. Mater. 17 (2008) 080–1088.
[157] N.A. Braga, C.A.A. Cairo, E.C. Almeida, M.R. Baldan, N.G. Ferreiraa, Diam. Relat. Mater. 17 (2008) 1891–1896.

[158] L. Yang, B.W. Sheldon, T.J. Webster, Biomaterials 30 (2009) 3458–3465.
[159] J.J. Norman, T.A. Desai, Ann. Biomed. Eng. 34 (2006) 89–101.
[160] S.W. Lee, B.K. Oh, R.G. Sanedrin, K. Salaita, T. Fujigaya, C.A. Mirkin, Adv. Mater. 18 (2006) 1133–1136.
[161] J.Y. Yang, Y.C. Ting, J.Y. Lai, H.L. Liu, H.W. Fang, W.B. Tsai, J. Biomed. Mater. Res. 90A (2008) 629–640.
[162] W.B. Tsai, Y.C. Ting, J.Y. Yang, J.Y. Lai, H.L. Liu, J. Mater. Sci.-Mater. M 20 (2009) 1367–1378.
[163] R.C. Schmidt, K.E. Healy, J. Biomed. Mater. Res. 90A (2009) 1252–1261.
[164] K. von der Mark, J. Park, S. Bauer, P. Schmuki, Cell. Tissue Res. 339 (2010) 131–153.
[165] D. Khang, M. Sato, R.L. Price, T.J. Webster, Int. J. Nanomed. 1 (2006) 65–72.
[166] D. Khang, G.E. Park, T.J. Webster, J. Biomed. Mater. Res. 86A (2008) 253–260.
[167] J.Y. Kim, D. Khang, J.E. Lee, T.J. Webster, J. Biomed. Mater. Res. 88A (2009) 419–426.
[168] A. Reising, C. Yao, D. Storey, T.J. Webster, J. Biomed. Mater. Res. 87A (2008) 78–83.
[169] G.E. Park, M.A. Pattison, K. Park, T.J. Webster, Biomaterials 26 (2005) 3075–3082.
[170] T.W. Chung, D.Z. Liu, S.Y. Wang, S.S. Wang, Biomaterials 24 (2003) 4655–4661.
[171] S.Y. Chou, P.R. Krauss, P.J. Renstrom, Appl. Phys. Lett. 67 (1995) 3114–3116.
[172] H.W. Li, W.T.S. Huck, Curr. Opin. Solid St. M. Sci. 6 (2002) 3–8.
[173] H.B. Lan, Y.C. Ding, H.Z. Liu, B.H. Lu, Microelectron. Eng. 84 (2007) 684–688.
[174] E.K.F. Yim, R.M. Reano, S.W. Pang, A.F. Yee, C.S. Chen, K.W. Leong, Biomaterials 26 (2005) 5405–5413.
[175] A.S.G. Curtis, N. Gadegaard, M.J. Dalby, M.O. Riehle, C.D.W. Wilkinson, G. Aitchison, IEEE T. Nanobiosci. 3 (2004) 61–65.
[176] X.F. Feng, J. Zhang, H.K. Xie, Q.H. Hu, Q. Huang, W.W. Liu, Surf. Coat. Tech. 171 (2003) 96–100.
[177] M.R. Yang, K.S. Chen, J.L. He, Mater. Chem. Phys. 48 (1997) 71–75.
[178] J.C. Lin, Y.F. Chen, C.Y. Chen, Biomaterials 20 (1999) 1439–1447.
[179] C.S. Kwok, T.A. Horbett, B.D. Ratner, J. Control. Release 62 (1999) 301–311.
[180] S.K. Hendricks, C. Kwok, M.C. Shen, T.A. Horbett, B.D. Ratner, J.D. Bryers, J. Biomed. Mater. Res. 50 (2000) 160–170.
[181] Y. Yuan, C.S. Liu, Y. Zhang, M. Yin, C.O. Shi, Surf. Coat. Tech. 201 (2007) 6861–6864.
[182] W. Zhang, Y.J. Luo, H.Y. Wang, J. Jiang, S.H. Pu, P.K. Chu, Acta Biomater. 4 (2008) 2028–2036.
[183] H.Y. Wang, D.T.K. Kwok, W. Wang, Z.W. Wu, L.P. Tong, Y.M. Zhang, P.K. Chu, Biomaterials 31 (2010) 413–419.